EUROPEAN RESPIRATORY *journal*

FLAGSHIP SCIENTIFIC JOURNAL OF ERS

Early View

Original article

Mitochondrial antiviral signalling protein is crucial for the development of pulmonary fibrosis

Sang-Hun Kim, Jung Yeon Lee, Chang Min Yoon, Hyeon Jun Shin, Sei Won Lee, Ivan Rosas, Erica Herzog, Charles Dela Cruz, Naftali Kaminski, Min-Jong Kang

Please cite this article as: Kim S-H, Lee JY, Yoon CM, *et al*. Mitochondrial antiviral signalling protein is crucial for the development of pulmonary fibrosis. *Eur Respir J* 2020; in press (https://doi.org/10.1183/13993003.00652-2020).

Mitochondrial antiviral signaling protein is crucial for the development of pulmonary fibrosis

Sang-Hun Kim[1], Jung Yeon Lee[1], Chang Min Yoon[1], Hyeon Jun Shin[1], Sei Won Lee[2], Ivan Rosas[3], Erica Herzog[1], Charles Dela Cruz[1], Naftali Kaminski[1] and Min-Jong Kang[1] †

[1] Section of Pulmonary, Critical Care and Sleep Medicine, Department of Internal Medicine, Yale University School of Medicine, New Haven, CT 06520-8057, USA

[2] Department of Pulmonary and Critical Care Medicine, and Clinical Research Center for Chronic Obstructive Airway Diseases, Asan Medical Center, University of Ulsan College of Medicine, Seoul, Korea

[3] Department of Medicine, Harvard University School of Medicine, Boston, MA 02115, USA

Take home message : This study provides proof-of-concept that MAVS may play a critical role in the development of pulmonary fibrosis and targeting MAVS or its signaling by proapoptotic BH3 mimetics may be considered as a feasible strategy for the treatment of IPF.

† Correspondence: min-jong.kang@yale.edu

Abstract

Danger signals, or damage- associated molecular patterns (DAMPs), instigate mitochondrial innate immune responses wherein Mitochondrial Antiviral Signaling protein (MAVS) functions as a key platform molecule to mediate them. The role of MAVS in the pathogenesis of idiopathic pulmonary fibrosis (IPF), however, has not been identified yet. A possibility whether the MAVS signaling can be modulated by currently existing drugs has not been explored, either. Here, using an established model of pulmonary fibrosis, we demonstrate that MAVS plays as a critical mediator of multiple DAMPs signaling pathways and the consequent lung fibrosis after bleomycin-induced injury *in vivo*. After bleomycin injury, the expression of MAVS was mainly observed in macrophages. In addition, multimeric MAVS aggregation, a key event of MAVS signaling activation, was significantly increased and persisted in bleomycin-injured lungs. Interestingly, a proapoptotic BH3 mimetic ABT-263 attenuated the expression of MAVS and its signaling and, consequently, the development of experimental pulmonary fibrosis. In contrast, the therapeutic effects of Pirfenidone or Nintedanib, two approved drugs for IPF treatment, were not related to the modulation of MAVS or its signaling. Importantly, multimeric MAVS aggregation was significantly increased in lungs from the patients with IPF as well. In conclusion, MAVS may play an important role in the development of pulmonary fibrosis, and targeting MAVS with BH3 mimetics may provide a novel therapeutic strategy for IPF, a major unmet disorder.

Words Count: 223

Introduction

Idiopathic pulmonary fibrosis (IPF) is defined as a specific form of chronic, progressive, fibrosing interstitial pneumonia of unknown cause and is characterized by the histopathologic and/or radiologic pattern of usual interstitial pneumonia (UIP) [1]. IPF is a fatal lung disease. Patients of this disorder are destined to suffer an unpredictable decline of lung function with a lower survival rate and often die from respiratory insufficiency within 2-5 years of diagnosis [1-3]. As such, it is a major unmet medical need in human health and requires better mechanistic understanding of pathogenesis to develop novel disease-modifying therapeutics.

Mitochondrial function and behavior have been highlighted to be fundamental to the physiology of cellular and organismal health; consequently, "mitochondrial dysfunction" has been implicated in a wide range of diseases that encompass all aspects of health and disease [4-7]. In accordance with the recent evolution of our understanding of the mitochondrial role in human health, increasing attention has been paid to the functional roles of mitochondrial molecules and their underlying mechanisms by which they may contribute to the pathogenesis of IPF [8-10].

During tissue injury or damage responses, mitochondrial functions are influenced responding to intracellular perturbations. The alteration of mitochondrial functions, in turn, modulates various intracellular signaling in order to execute appropriate cellular functions [11]. Mitochondrial antiviral signaling protein (MAVS) represents such an example and functions as a platform molecule to mediate mitochondrial innate immune signaling [12-14]. The role of MAVS contributing to IPF pathogenesis wherein dysregulated tissue damage responses play an important role, however, has not been identified yet. In addition, a possibility whether the MAVS

signaling can be modulated by currently existing drugs in order to offer a novel therapeutic strategy has not been explored, either.

Here, we demonstrate that MAVS plays a critical role in the development of experimental pulmonary fibrosis after bleomycin-induced lung injury *in vivo*, an established mammalian model of IPF. Bleomycin-induced fibrotic responses and multiple DAMPs signaling pathways were significantly attenuated via a MAVS-dependent manner in murine lungs *in vivo*. In addition, bleomycin-induced cellular senescence was significantly attenuated in MAVS-deficiency. Intriguingly, the BH3 (B-cell lymphoma 2 (Bcl-2) Homology 3) mimetic ABT-263 induced a significant reduction of the MAVS signaling and, consequently, attenuated the development experimental pulmonary fibrosis in our model. In contrast, the therapeutic effects of Pirfenidone or Nintedanib, respectively, the currently approved drugs known to decelerate IPF progression, were not related to the MAVS signaling. Finally, human studies revealed a significant activation of MAVS in lungs from the patients with IPF compared to those of controls. Taken together, these data suggest that MAVS and its mitochondrial innate immune signaling, which can be modulated by BH3 mimetics, is activated and may play an important role in the pathogenesis of IPF.

Materials and Methods

Animals and experimental design

Wild type (WT, *Mavs*$^{+/+}$) (from Jackson Laboratories) and *Mavs*$^{-/-}$ (from Dr. Z. J. Chen, University of Texas) were all kept on C57BL/6J background and bred at Yale University Animal Facility. All animal experiments were approved by the Yale Animal Care and Use Committee

(YACUC). An established mammalian model of idiopathic pulmonary fibrosis (IPF) was utilized as described in previous publications [15, 16]. Briefly, to induce a pulmonary fibrosis, mice were treated with bleomycin (Pfizer, #NDC 61703-0332-18) with phosphate buffered saline (PBS) by intra-tracheal administration or oropharyngeal aspiration, respectively. At designated time points after bleomycin administration, mice were euthanized with urethane by intraperitoneally injection, hearts were perfused with PBS, and lungs were harvested for further analyses. For BAL collection, the trachea was cannulated and lavaged two times with 0.9 ml PBS. Samples were centrifuged at 1,500 rpm for 5 min, and the cell-free supernatants were collected for ELISA assay. The cell pellets were recovered in 200 μl sterile PBS, and total cell count of BAL was done using automated cell count using a Coulter Analzer (Beckman Coulter, Brea, CA).

Therapeutic drugs treatment.

To test the therapeutic efficacy of various existing drugs in our modeling of IPF, ABT-263 (40 mg/kg; MedChemExpress), pirfenidone (40 mg/kg; MedChemExpress), nintedanib (40 mg/kg; MedChemExpress) or vehicle controls (5% tween-80), respectively, were administered by intra-peritoneal injection at days 8, 10, 12, 14, 16, 18 and 20 after bleomycin administration, and the mice were sacrificed at day 21.

Human sample preparation

For the evaluation and comparison of MAVS aggregation in the patient with IPF or healthy controls, the lung tissue samples were obtained from Dr. Ivan Rosas' laboratory. Human lung explants were obtained from donations of patients who sign informed consent and undergo lung transplantation at the Brigham and Women's Hospital, or donor organs provided by the New

England Organ Bank and/or the National Disease Research Interchange (NDRI). The study's protocol was approved by the Partners Healthcare Institutional Board Review (IRB Protocol # 2011P002419). Briefly, lungs were sliced and washed with cold sterile PBS several times. Visible airway structures, vessels, blood clots and mucin were removed. Tissues were minced mechanically into small pieces (<5 mm) and then incubated for 45 minutes in 37°C within the digestion medium, which consist of 30 U/ml elastase (Elastin Products Company, Owensville, MO), 0.2 mg/ml DNAse I (Sigma, St. Louis, MO), 0.3 mg/ml liberase (Roche, Basel, Switzerland) and 1% Penicillin/Streptomycin diluted in DMEM/F12 medium (Lonza, Basel, Switzerland). Digested tissues were filtered using a metal strainer (Sigma). Unfiltered tissues were incubated a second time in digestion medium for 30 minutes or less, followed by repeat filtration and addition of 10% FBS to stop the enzymatic reaction. Flow-through from both filtrations was combined and centrifuged at 600G, 4°C for 10 minutes. The pellet was resuspended in red cell lysis buffer (VWR, Radnor, PA) for <5 minutes in 37°C and centrifuged again. The pellet was resuspended in DMEM/F12 medium and filtered using a 100 μm strainer (Fisher Scientific, Waltham, MA). Freezing medium (10% FBS and 10% DMSO in DMEM/F12) was then added to the filtrate. Cell suspensions were aliquoted and stored in liquid nitrogen for future SDD-AGE or BN-PAGE applications.

Statistical analysis

All statistical analysis was executed using the Prism (GraphPad, version 6) software program. Comparisons between two groups were performed with Student *t* test (unpaired). For the multiple comparisons, 2-way ANOVA was used. The significance of survival rate was

analyzed with the log-rank test. Values are expressed as mean ± SEM, SD or Min to Max. Statistical significance was defined at a level of *P* less than 0.05.

Additional experimental methods were described in Supplementary Information; these methods include (a) Sircol assay, (b) Flow cytometric analysis, (c) Histology, immunohistochemistry and immunofluorescence, (d) Isolation of murine alveolar macrophages, (e) ELISA, (f) qRT-PCR, (g) Western blot analysis, (h) Quantification of cell-free double-stranded DNA, (i) Mitochondrial isolation, (j) Blue Native-Polyacrylamide Gel Electrophoresis (BN-PAGE) and Semi-Denaturing Detergent-Agarose Gel Electrophoresis (SDD-AGE), (k) *In vitro* cell culture, and (l) Isolation and culture of mouse lung fibroblasts and mouse embryonic fibroblasts

Results

MAVS plays a crucial role in lung fibrosis after bleomycin administration *in vivo*.

In these studies, we questioned whether MAVS, a novel adaptor molecule of mitochondrial innate immune signaling, may have a functional role in the pathogenesis in a mammalian model of experimental pulmonary fibrosis. When 1.5 unit amount (U)/kilogram of body weight (kg) of bleomycin was administered to male and female mice, respectively, via intra-tracheal (IT) delivery, the bleomycin-induced tissue injury responses revealed striking difference between two groups of C57BL/6J wild type (WT) or MAVS null mutants ($^{-/-}$) mice. Specifically, all mice from WT controls were dead while 9 of 14 (64%) mice survived among *Mavs*$^{-/-}$ group (Figure 1a). With 1.0 U/kg of bleomycin dose, more than half of WT mice were dead while all *Mavs*$^{-/-}$ mice

survived (Figure 1b). With 0.4 U/kg of bleomycin dose via IT delivery, we obtained about 3-fold increase of total lung collagen contents, which is comparable to known publications (Figure 1c) [8, 9]. Hence, 0.4 U/kg of bleomycin was administered via IT delivery for all the following *in vivo* experiments, if not specified. Bleomycin-induced pulmonary fibrosis and loss of body weight, respectively, were significantly ameliorated in the lung from *Mavs*$^{-/-}$ mice compared to those of WT controls (Figure 1c and d). These observations were confirmed by histologic evaluations (Figure 1e and Figure S1a). A similar level of the reduction of fibrotic response was observed between male and female groups of mice (data not shown). Immunohistochemistry (IHC) and immunofluorescence evaluations demonstrated significant staining of MAVS molecule after bleomycin administration and the staining was observed most prominently in macrophages but not restricted to this cell population (Figure 1f, g and S1a). Flow cytometric evaluation revealed that $CD45^{+}F4/80^{+}$ cells occupied about 80 % of the lung cells which were stained with anti-MAVS antibody after bleomycin treatment (Figure 1h). The specificity of MAVS staining in our imaging studies as well as our flow cytometric evaluation were presented (Figure S1b and c). The identification of specific cell types and the gating strategy of our flow cytometric evaluation were undertaken following the methods as reported in the literatures (Fig S1d) [17, 18]. To determine whether the bleomycin-induced tissue injury *in vivo* is altered in the presence or absence of MAVS, the quantification of Terminal deoxynucleotidyl transferase dUTP nick end labeling (TUNEL) assay and the evaluation of the active form of caspase-3, a marker of apoptotic cell death, were undertaken in the lungs of WT and $MAVS^{-/-}$ mice. The lungs were obtained at the time point of Day 3 and Day 5, respectively, after the administration of bleomycin *in vivo*. Indeed, these results revealed that the bleomycin-induced tissue injury *in vivo* was not attenuated in MAVS deficiency (Fig S1e – g). Overall, these data reveal that MAVS

is expressed mainly in pulmonary macrophages and plays an important pathogenic role in a mammalian IPF model.

MAVS-dependent fibrogenic responses in bleomycin-induced pulmonary fibrosis

Next, the experiments were undertaken to determine the role of MAVS in regulating TGF-β signaling, often regarded as the master regulator of tissue fibrosis, as well as the consequent fibrogenic responses. Initially, the bleomycin-induced induction of total and active TGF-β seemed to be attenuated but didn't reach statistical significance in the lung from *Mavs*$^{-/-}$ mice compared to those of WT controls (Figure 2a and b). For accurate determination of this statistical significance, additional experiments were undertaken with increased numbers of mice. Indeed, the results revealed that the bleomycin-induced induction of total and active TGF-β, respectively, was significantly attenuated in MAVS deficiency *in vivo* (Figure 2c and d). In addition, when their gene expressions were evaluated for the molecules involved in TGF-β superfamily signaling, the mRNA expressions of connective tissue growth factor (*Ctgf*) and interleukin (IL)-13 (*Il13*), respectively, were significantly attenuated in MAVS deficiency (Fig S2a – f). Both *Ctgf* and *Il13* have also been identified to regulate the phosphorylation status of Smad2/3, a critical event in TGF-β super family signaling [19-21]. Intra-alveolar inflammatory response was not significantly altered between the two groups (Figure S2g). Additional evaluations of molecular markers which are known to be differentially expressed in macrophages during distinct types of classical, alternative and fibrotic/reparative activations, respectively, didn't reveal specific differences between the two groups, either (Figure S2h). Importantly, Western blot evaluation of the activation status of SMAD-2/3, canonical markers of TGF-β distal signaling molecules, revealed the marked attenuation in MAVS deficiency (Figure 2e).

Moreover, well-known marker molecules of tissue fibrotic responses were significantly altered via a MAVS-dependent manner. Specifically, the molecular expressions of *Fibronectin*, Alpha-smooth muscle actin (*α-Sma*) and Collagen 1α (*Col1α*), respectively, which were induced after bleomycin injury, were markedly attenuated in MAVS-deficient lungs (Figure 2f - i). These observations were further validated by the densitometry evaluations of these molecules (Fig S2g – j). In addition, IHC evaluation of Col1α confirmed the above findings, revealing that bleomycin injury-induced expression of Col1α was markedly attenuated in lung tissues from *Mavs*$^{-/-}$ mice (Figure 2j). Collectively, these data suggest that MAVS-dependent and independent distinct mechanisms exist for the pathogenesis of pulmonary fibrosis in our model.

MAVS amplifies multiple DAMPs signaling during fibrotic phase after bleomycin injury

The above findings intrigued us to investigate how MAVS may play a crucial role in the development of experimental pulmonary fibrosis although the induction of total and active TGF-β are not significantly altered. Paying our attention to the fact that MAVS determines even organismal death or survival after severe bleomycin injury, experiments were undertaken to investigate whether DAMPs signaling is regulated via a MAVS-dependent manner after bleomycin injury. Indeed, multiple molecules related to various DAMPs signaling pathways were induced via a time-kinetic manner after bleomycin injury *in vivo* (Figure 3a - g). It is noteworthy that the measurement of cell-free dsDNA amount in bronchoalveolar lavage (BAL) fluid revealed the significant increase after bleomycin injury *in vivo* (Figure 3g). Interestingly, among these multiple molecules, dsDNA, cGAS and STING, respectively, were significantly attenuated via a MAVS-dependent manner after bleomycin injury *in vivo* (Figure 3h - i). Recently, polymerization of STING was identified as a critical event of its activation [22].

Indeed, its evaluation by the application of semi-denaturing detergent agarose gel electrophoresis (SDD-AGE) revealed a significant induction of STING aggregation at day 14, a time-point often regarded as the peak of fibrogenesis in our IPF murine modeling (Figure 3j). Intriguingly, the bleomycin-induced STING aggregation was markedly attenuated in MAVS-deficient lungs (Figure 3j). Similar observations were further accentuated in a higher dose (1.0 U/kg) of bleomycin injury *in vivo*. Specifically, the expression of additional molecules of DAMPs signaling pathways including *Sting*, *Hmgb1*, *Nlrp3* and purinergic receptor P2Y2 (*P2ry2*) molecules was significantly attenuated in MAVS-deficient lungs with the higher dose (1.0 U/kg) (Figure S3a - d). In accordance with this, bleomycin injury-induced induction of dsDNA amount from BAL fluid as well as cGAS protein and STING aggregation were also significantly attenuated via a MAVS-dependent manner in this high dose (1.0 U/kg) (Figure S3e - g). Taken together, these results suggest that multiple DAMPs signaling pathways, which are induced or activated by bleomycin injury *in vivo* and persist during the fibrotic phase of IPF murine modeling, are critically regulated via a MAVS-dependent manner.

A proapoptotic BH3 mimetic ABT-263 inhibits MAVS and lung fibrosis *in vivo*.

While we were undergoing experiments to define the role of apoptosis in the regulation of DAMPs signaling in our system, surprisingly, we observed a previously unidentified effect of proapoptotic BH3 mimetics. Specifically, BH3 mimetic drugs could reduce the MAVS expression. In murine lung epithelial-12 (MLE 12) cells, when several BH3 mimetics including ABT-263 (a Bcl-2 and Bcl-xl inhibitor), ABT-199 (a Bcl-2 inhibitor) and A1155483 (a Bcl-xl inhibitor), respectively, were treated after bleomycin injury *in vitro*, we noticed that the expression of MAVS molecule was significantly reduced (Figure 4a and b). In addition, the

ABT-263-induced reduction of MAVS was not related to the decrease of mitochondrial proteins; the components of mitochondrial oxidative phosphorylation (OXPHOS) were not altered in our experiments (Figure 4b). A similar finding was observed when we expanded the evaluation to different types of primary cells including murine embryonic fibroblasts (MEFs), peritoneal macrophages (PMs), as well as primary mouse lung fibroblasts (MLF) cells, respectively (Figure 4c - e). Inspired by these observations, a pharmacologic approach *in vivo* was undertaken in order to evaluate potential therapeutic effects of ABT-263 in our murine pulmonary fibrosis model (Figure 4f). Specifically, from day 8 after bleomycin injury *in vivo*, ABT-263 (40mg/kg of body weight) was treated by intraperitoneal administration every other day and the fibrotic responses were evaluated. Indeed, the bleomycin-induced increase of total lung collagen contents was significantly attenuated with ABT-263 treatment *in vivo* (Figure 4f and S4). In line with this, Western blot evaluation revealed that the activation status of SMAD-2/3, the expression of Fibronectin, as well as the expression of α-SMA, respectively, were significantly ameliorated with ABT-263 treatment *in vivo* (Figure 4g). These observations were supported by *in vitro* experiments. In MEF, MLF and normal human lung fibroblasts (NHLF) cells, respectively, TGF-β1-induced activation of SMAD-2/3 was significantly reduced after ABT-263 treatment *in vitro* (Figure 4h). Overall, these results provide compelling evidence that the BH3 mimetic ABT-263 can attenuate the expression of MAVS and, consequently, the development of experimental pulmonary fibrosis.

Therapeutic effects of Pirfenidone or Nintedanib are not related to MAVS.

To date, Pirfenidone and Nintedanib are the only approved drugs known to decelerate the disease progression of IPF [23, 24]. However, it has not been known whether these drugs can

modulate MAVS signaling *in vitro* or *in vivo*. When *in vitro* experiments were undertaken to address this issue, these two drugs failed to reduce the expression of MAVS while ABT-263 can significantly reduce it (Figure 5a and b). Overall mitochondrial proteins such as the OXPHOS components were not altered in our experiments after the treatment of these drugs (Figure 5b). Next, when the therapeutic effects of these drugs in our IPF modeling system were compared, the bleomycin-induced increase of total lung collagen contents as well as semi-quantitative severity scores of the microscopic changes were significantly ameliorated after treatment with these three drugs, respectively (Figure 5c, d and Figure S5). No statistical difference was noted between the three groups (Figure 5c and d, * note: Two mice were dead during the fibrotic phase in the Nintedanib treatment group). In line with this, Western blot evaluation revealed that the activation status of SMAD-2/3, the expression of Fibronectin, as well as the expression of α-SMA, respectively, were significantly ameliorated with the treatment of these three drugs, respectively (Figure 5e). Overall, these data suggest that the pharmacologic effects of Pirfenidone or Nintedanib, respectively, for the treatment of IPF are not directly related to MAVS.

Bleomycin-induced cellular senescence is inhibited in MAVS deficiency.

Cellular senescence has recently emerged as a key driving force of IPF pathogenesis [25, 26]. In addition, ABT263 has been identified to mediate anti-fibrotic effects via its selective removal of senescent cells due to the induction of their apoptotic cell death, called senolysis [25]. Thus, experiments were undertaken to further determine how ABT263-induced senolytic effect might be related to the molecular function of MAVS in cellular senescence. From MEF cells, bleomycin-induced cellular senescence, which was evaluated by the measurement of SA-β-Gal

activity, was significantly attenuated after treatment with ABT-263 (Figure 6a and b). As expected, the reduction of cellular senescence was related to the induction of apoptosis and the consequent decrease of cell viability via a dose-dependent manner (Figure 6c, d and data not shown). Notably, a significant reduction of the MAVS protein expression was observed in association with the ABT263-induced senolysis (Figure 6d). Similar results were obtained from MLE12 cells, further confirming the reduction of MAVS in association with ABT263-mediated senolysis (Figure S6a – d). Next, in order to clarify whether the inhibitory effect of ABT263 on regulation of MAVS protein expression is mainly related to its selective removal of senescent cells (senolysis) in the setting of cellular senescence or whether ABT263 may mediate its inhibitory effect on MAVS via a senolysis-independent mechanism, further experiments with no stimulation of bleomycin were undertaken, eliminating the bleomycin-induced cellular senescence. Interestingly, after treatment with ABT263, a significant reduction of MAVS protein was observed from all three different cell types tested in this setting (Figure 6e – g). Finally, to define the functional role of MAVS which may play in bleomycin-induced cellular senescence *in vitro*, when SA-β-Gal activity was evaluated and compared in the presence or absence of MAVS, the bleomycin-induced cellular senescence was significantly attenuated in MAVS deficiency (Figure 6h & i). Intriguingly, the level of apoptotic cell death or cell viability was not significantly different in the presence or absence of MAVS (Figure 6j and data not shown), revealing that the reduction of bleomycin-induced cellular senescence in MAVS deficiency cannot be attributed to senolysis. Rather, these results demonstrate that the bleomycin-induced cellular senescence is inhibited in MAVS deficiency. The functional significance of MAVS in the regulation of bleomycin-induced senescence was also evaluated in our *in vivo* model. When gene expressions of known senescence markers were evaluated, $P16^{INK4a}$, $P19^{ARF}$ and $P21^{Cip1}$

mRNAs, respectively, were significantly induced in our murine pulmonary fibrosis model (Figure S6e-g). Indeed, the bleomycin injury-induced mRNA expressions of *P16*^{INK4a} and *P19*^{ARF}, respectively, were significantly attenuated in a MAVS-dependent manner (Figure 6k and l). In accordance with the time-kinetic patterns of its mRNA expressions, the P16^{INK4a} protein expression was significantly induced, reaching the peak of its expression at day 14 after bleomycin injury *in vivo* (figure S6h). Importantly, the induction of P16^{INK4a} protein was significantly reduced in MAVS deficiency at day 14 and day 21, respectively, after bleomycin administration *in vivo* (Figure 6m and S6i). Collectively, these results suggest that, in addition to its known senolytic effect, ABT263 may exert its anti-fibrotic effects by the reduction of MAVS. In addition, MAVS may play a functional role in the induction of bleomycin-induced cellular senescence.

Multimeric aggregation of MAVS, a critical event of MAVS signaling, is significantly activated in humans as well as in mice

Because prion-like multimeric aggregation of MAVS molecules on mitochondrial outer membrane was identified as a critical event for its proper signaling [27], experiments were undertaken to evaluate this in our system. Indeed, SDD-AGE as well as blue native-polyacrylamide gel electrophoresis (BN-PAGE) evaluation revealed that bleomycin injury induces a significant MAVS aggregation *in vivo* (Fig 7a). This observation could be observed from mitochondrial fraction and whole lung lysates as well (Figure 7a). Surprisingly, this phenomenon persisted even at day 14 after bleomycin administration. An additional finding was noted in our experiments. Although the expression of MAVS was shown to be markedly enhanced after bleomycin administration in IHC evaluation (Figure 1e), the absolute amount of

MAVS protein in the lung tissues seemed to be decreased during bleomycin-induced fibrogenesis *in vivo* (Figure 7a). We interpret the data as additional evidence for supporting the multimeric aggregation of MAVS during fibrogenesis. Specifically, the strong positive staining of MAVS obtained from IHC evaluation as demonstrated in Figure 1E may reflect the multimeric aggregation of MAVS which is not related to its molecular induction after bleomycin injury *in vivo*. Next, when the experiments were undertaken whether the bleomycin-induced multimeric aggregation of MAVS *in vivo* can be modulated by ABT-263, Pirfenidone or Nintedanib, respectively, intriguingly, the multimeric aggregation of MAVS was markedly attenuated only after ABT-263 treatment (Figure 7b and c). Among multiple drugs tested, all BH3 mimetics could ameliorate the multimeric aggregation of MAVS (Figure 7d). In contrast, Pirfenidone or Nintedanib, respectively, failed to ameliorate it (Figure 7d). Finally, in order to determine the clinical relevance of the above finding observed in murine disease modeling, the experiment was undertaken to test whether MAVS aggregation is observed in the lung tissues from human patients with IPF. Indeed, significant increase of MAVS aggregation was observed from 11 patients among 13 specimens from IPF patients, while only two specimens showed MAVS aggregation among 9 controls, demonstrating a compelling statistical significance (Figure 7e and f, $^{**}p < 0.01$). Overall, these data demonstrate that persistent MAVS aggregation, a key event of MAVS signaling activation, is observed in lungs from the patients with IPF as well as in our mammalian model of IPF, and, importantly, can be therapeutically targeted by BH3 mimetics.

Discussion

The current studies are novel as they demonstrate that (i) MAVS, a key adaptor of mitochondrial innate immune signaling, is significantly activated after fibrogenic injury; (ii) the activation of MAVS is associated with various DAMPs signaling pathways, especially, cGAS-STING innate immune signaling; (iii) proapoptotic BH3 mimetics can reduce the MAVS expression as well as its multimeric aggregation; and most importantly, (iv) the multimeric aggregation of MAVS, a key event during MAVS signaling activation, is markedly enhanced in lungs from the patients with IPF. Overall, these studies suggest that MAVS plays a critical pathogenic role in experimental pulmonary fibrosis.

As the first mitochondria-localized protein to be linked to innate immunity [12], MAVS has been identified to be involved in multiple biological phenomena including mitochondrial innate immune signaling, apoptosis, autophagy and metabolic functions [28-30]. Given that recent studies are continuously highlighting the functional roles of mitochondria and their underlying mechanisms by which mitochondrial dysfunction contributes to the pathogenesis of IPF [6, 31], the current studies emphasize mitochondrial significance by illuminating the role of MAVS-mediated DAMPs signaling in fibrotic tissue injury/damage responses.

Danger theory has been implicated in the pathogenesis of many chronic disorders for which effective therapeutics are not available, thus remaining major unmet medical needs [32-34]. IPF is such an example. Intriguingly, MAVS, a molecule mostly studied in the context of viral PAMPs signaling, is significantly activated by bleomycin-induced injury which is obviously not related to viral infection. In addition, persistent MAVS aggregation is observed in the lungs from

IPF patients. Fibrogenic tissue injury may drive fibrosis by inducing various endogenous DAMPs signaling which could be converged to MAVS. A potential significance of MAVS signaling in the pathogenesis of non-viral injury-induced chronic diseases was reported in another publication [35].

The phosphorylation state of receptor-regulated Smads (R-Smads) such as Smad2/3 determines the most critical event in TGF-β super family signaling (reviewed in Reference [36]). Importantly, multiple TGF-β-dependent and -independent complex regulatory mechanisms have been identified to ensure their phosphorylation status as a dynamic and tightly controlled event (reviewed in References [36, 37]). Our current study adds further knowledge to this important research area, by revealing the regulation of R-Smads phosphorylation via a MAVS-dependent manner. In addition, it has rarely been reported whether MAVS may play a role in cellular senescence. By demonstrating that bleomycin injury-induced cellular senescence is significantly attenuated in a MAVS-dependent manner, our study may provide additional mechanistic insight of how MAVS contributes to the development of pulmonary fibrosis. The significance of these novel observations should be explored in future studies, considering that cellular senescence has emerged as a crucial driving force of IPF pathogenesis [25, 26, 38].

In line with our studies, a recent study demonstrated a potential efficacy of targeting myofibroblast antiapoptotic proteins with BH3 mimetic drugs in skin fibrosis [39]. In addition, the pharmacologic effects of BH3 mimetics that can selectively remove senescent cells, called senolysis, have recently been highlighted to have therapeutic potential for the treatment of age-associated diseases [40, 41]. Regarding this, our finding that BH3 mimetics can attenuate the MAVS expression *in vitro* and *in vivo* might open up new vistas for the underlying mechanisms by which BH3 mimetics function as novel therapeutics. Specifically, when combined with the

inhibitory role of MAVS in regulating multiple DAMPs signaling as well as cellular senescence, the current study enables us to speculate that BH3 mimetics might take its antifibrotic effects by inhibiting MAVS and the consequent DAMPs signaling pathways for the treatment of fibrosis, in addition to their known senolytic effects [40]. Or, the senolytic effects of BH3 mimetics might be linked to their inhibitory function on MAVS through an intricate regulatory network. Importantly, these questions about senescence or non-senescence impact of BH3 mimetics on the regulation of fibrosis, especially in relation to their inhibitory function on MAVS, have rarely been explored. Our novel observations cast intriguing mechanistic questions to explore therapeutic potential that BH3 mimetics may have for the treatment of fibrotic disorders including IPF in humans.

To date, Pirfenidone and Nintedanib are the only approved drugs known to decelerate the disease progression of IPF [23, 24]. Pirfenidone is known to mediate its antifibrotic effects via its anti-oxidant, anti-fibrotic and anti-inflammatory properties [42]. Nintedanib is a multi-tyrosine kinase inhibitor and is known to inhibit the receptor kinases of platelet-derived growth factor (PDGF), fibroblast growth factor (FGF) and vascular endothelial growth factor (VEGF), which are all thought to play an important role in the pathogenesis of IPF [24]. However, their modulatory effects on the expression of MAVS or its-mediated DAMPs signaling have not been explored yet. Although this question has not been investigated in a comprehensive manner, our studies suggest that therapeutic effects of Pirfenidone or Nintedanib, respectively, for the treatment of IPF, are not related to the modulation on MAVS and its signaling.

Several issues remain unanswered in the current studies. Detailed mechanistic explanations are not provided about how endogenous DAMPs-mediated innate immune signaling pathways may contribute to the pathogenesis of IPF. The molecular action mechanism(s) by which

proapoptotic BH3 mimetics function to reduce the MAVS expression and its aggregation has not been investigated, either. In addition, an interesting question is raised about whether synergistic therapeutic effects will be observed if a BH3 mimetic is combined together with Pirfenidone or Nintedanib, respectively, for the IPF treatment. Future studies will be required to explore these important questions.

Although bleomycin-induced experimental fibrosis modeling may not fully recapitulate the pathogenesis of human IPF, multimeric aggregation of MAVS was markedly observed in the lungs of the patients with IPF as well as the late fibrotic phase in our experimental modeling. We believe that a similar observation of multimeric MAVS aggregation in humans as well as in our murine model highlights a potential significance of MAVS in IPF pathogenesis. An enhanced understanding of MAVS and its signaling in fibrotic tissue injury or damage responses may bring a significant impact on overall fibrosis biology including IPF.

In conclusion, these studies demonstrate that MAVS plays an important role in the development of experimental pulmonary fibrosis in a mammalian model of IPF, and provide a rationale that targeting MAVS or its signaling may be considered as a feasible strategy for the regulation of pulmonary fibrosis.

Acknowledgments

The authors thank Ms. Susan Ardito for excellent administrative assistance. These studies were supported by NHLBI R01HL130283 (MJK) and NIA R01AG053495 (MJK).

Author contributions

Conceived the idea and designed the experiments (SHK, JYL, MJK); Performed experiments (SHK, JYL, HJS, CMY, SWL); Provided important reagents/tools (SWL, CMY, IR, NK); Provided scientific insight (SHK, EH, CDC, NK, MJK); Analyzed data (SHK, EH, MJK); Drafted the manuscript (SHK, JYL, MJK); All of the authors reviewed the manuscript.

Conflict of interest

The authors declare no competing financial interests.

References

1. Raghu G, Collard HR, Egan JJ, Martinez FJ, Behr J, Brown KK, Colby TV, Cordier JF, Flaherty KR, Lasky JA, Lynch DA, Ryu JH, Swigris JJ, Wells AU, Ancochea J, Bouros D, Carvalho C, Costabel U, Ebina M, Hansell DM, Johkoh T, Kim DS, King TE, Jr., Kondoh Y, Myers J, Muller NL, Nicholson AG, Richeldi L, Selman M, Dudden RF, Griss BS, Protzko SL, Schunemann HJ, Fibrosis AEJACoIP. An official ATS/ERS/JRS/ALAT statement: idiopathic pulmonary fibrosis: evidence-based guidelines for diagnosis and management. *American journal of respiratory and critical care medicine* 2011: 183(6): 788-824.
2. Wolters PJ, Collard HR, Jones KD. Pathogenesis of idiopathic pulmonary fibrosis. *Annu Rev Pathol* 2014: 9: 157-179.
3. Hutchinson JP, McKeever TM, Fogarty AW, Navaratnam V, Hubbard RB. Increasing global mortality from idiopathic pulmonary fibrosis in the twenty-first century. *Annals of the American Thoracic Society* 2014: 11(8): 1176-1185.
4. Nunnari J, Suomalainen A. Mitochondria: in sickness and in health. *Cell* 2012: 148(6): 1145-1159.
5. Dela Cruz CS, Kang MJ. Mitochondrial dysfunction and damage associated molecular patterns (DAMPs) in chronic inflammatory diseases. *Mitochondrion* 2017.
6. Mora AL, Bueno M, Rojas M. Mitochondria in the spotlight of aging and idiopathic pulmonary fibrosis. *The Journal of clinical investigation* 2017: 127(2): 405-414.
7. Picard M, Wallace DC, Burelle Y. The rise of mitochondria in medicine. *Mitochondrion* 2016: 30: 105-116.
8. Bueno M, Lai YC, Romero Y, Brands J, St Croix CM, Kamga C, Corey C, Herazo-Maya JD, Sembrat J, Lee JS, Duncan SR, Rojas M, Shiva S, Chu CT, Mora AL. PINK1 deficiency impairs mitochondrial homeostasis and promotes lung fibrosis. *The Journal of clinical investigation* 2015: 125(2): 521-538.
9. Larson-Casey JL, Deshane JS, Ryan AJ, Thannickal VJ, Carter AB. Macrophage Akt1 Kinase-Mediated Mitophagy Modulates Apoptosis Resistance and Pulmonary Fibrosis. *Immunity* 2016: 44(3): 582-596.
10. Ryu C, Sun H, Gulati M, Herazo-Maya JD, Chen Y, Osafo-Addo A, Brandsdorfer C, Winkler J, Blaul C, Faunce J, Pan H, Woolard T, Tzouvelekis A, Antin-Ozerkis DE, Puchalski

JT, Slade M, Gonzalez AL, Bogenhagen DF, Kirillov V, Feghali-Bostwick C, Gibson K, Lindell K, Herzog RI, Dela Cruz CS, Mehal W, Kaminski N, Herzog EL, Trujillo G. Extracellular Mitochondrial DNA Is Generated by Fibroblasts and Predicts Death in Idiopathic Pulmonary Fibrosis. *American journal of respiratory and critical care medicine* 2017: 196(12): 1571-1581.

11. Chandel NS. Evolution of Mitochondria as Signaling Organelles. *Cell metabolism* 2015: 22(2): 204-206.

12. Seth RB, Sun L, Ea CK, Chen ZJ. Identification and characterization of MAVS, a mitochondrial antiviral signaling protein that activates NF-kappaB and IRF 3. *Cell* 2005: 122(5): 669-682.

13. Subramanian N, Natarajan K, Clatworthy MR, Wang Z, Germain RN. The adaptor MAVS promotes NLRP3 mitochondrial localization and inflammasome activation. *Cell* 2013: 153(2): 348-361.

14. Zevini A, Olagnier D, Hiscott J. Crosstalk between Cytoplasmic RIG-I and STING Sensing Pathways. *Trends Immunol* 2017: 38(3): 194-205.

15. Jiang D, Liang J, Hodge J, Lu B, Zhu Z, Yu S, Fan J, Gao Y, Yin Z, Homer R, Gerard C, Noble PW. Regulation of pulmonary fibrosis by chemokine receptor CXCR3. *The Journal of clinical investigation* 2004: 114(2): 291-299.

16. Yu G, Tzouvelekis A, Wang R, Herazo-Maya JD, Ibarra GH, Srivastava A, de Castro JPW, DeIuliis G, Ahangari F, Woolard T, Aurelien N, Arrojo EDR, Gan Y, Graham M, Liu X, Homer RJ, Scanlan TS, Mannam P, Lee PJ, Herzog EL, Bianco AC, Kaminski N. Thyroid hormone inhibits lung fibrosis in mice by improving epithelial mitochondrial function. *Nat Med* 2018: 24(1): 39-49.

17. Jurgensen HJ, Norregaard KS, Sibree MM, Santoni-Rugiu E, Madsen DH, Wassilew K, Krustrup D, Garred P, Bugge TH, Engelholm LH, Behrendt N. Immune regulation by fibroblasts in tissue injury depends on uPARAP-mediated uptake of collectins. *J Cell Biol* 2019: 218(1): 333-349.

18. Akamatsu T, Arai Y, Kosugi I, Kawasaki H, Meguro S, Sakao M, Shibata K, Suda T, Chida K, Iwashita T. Direct isolation of myofibroblasts and fibroblasts from bleomycin-injured lungs reveals their functional similarities and differences. *Fibrogenesis Tissue Repair* 2013: 6(1): 15.

19. Liu Y, Meyer C, Müller A, Herweck F, Li Q, Müllenbach R, Mertens PR, Dooley S, Weng HL. IL-13 induces connective tissue growth factor in rat hepatic stellate cells via TGF-β-independent Smad signaling. *Journal of immunology (Baltimore, Md : 1950)* 2011: 187(5): 2814-2823.

20. Ramazani Y, Knops N, Elmonem MA, Nguyen TQ, Arcolino FO, van den Heuvel L, Levtchenko E, Kuypers D, Goldschmeding R. Connective tissue growth factor (CTGF) from basics to clinics. *Matrix Biol* 2018: 68-69: 44-66.

21. Rodríguez-Vita J, Sánchez-López E, Esteban V, Rupérez M, Egido J, Ruiz-Ortega M. Angiotensin II activates the Smad pathway in vascular smooth muscle cells by a transforming growth factor-beta-independent mechanism. *Circulation* 2005: 111(19): 2509-2517.

22. Ergun SL, Fernandez D, Weiss TM, Li L. STING Polymer Structure Reveals Mechanisms for Activation, Hyperactivation, and Inhibition. *Cell* 2019: 178(2): 290-301 e210.

23. Noble PW, Albera C, Bradford WZ, Costabel U, du Bois RM, Fagan EA, Fishman RS, Glaspole I, Glassberg MK, Lancaster L, Lederer DJ, Leff JA, Nathan SD, Pereira CA, Swigris JJ, Valeyre D, King TE, Jr. Pirfenidone for idiopathic pulmonary fibrosis: analysis of pooled data from three multinational phase 3 trials. *The European respiratory journal : official journal of the European Society for Clinical Respiratory Physiology* 2016: 47(1): 243-253.

24. Wollin L, Wex E, Pautsch A, Schnapp G, Hostettler KE, Stowasser S, Kolb M. Mode of action of nintedanib in the treatment of idiopathic pulmonary fibrosis. *The European respiratory journal : official journal of the European Society for Clinical Respiratory Physiology* 2015: 45(5): 1434-1445.

25. Lehmann M, Korfei M, Mutze K, Klee S, Skronska-Wasek W, Alsafadi HN, Ota C, Costa R, Schiller HB, Lindner M, Wagner DE, Günther A, Königshoff M. Senolytic drugs target alveolar epithelial cell function and attenuate experimental lung fibrosis ex vivo. *The European respiratory journal : official journal of the European Society for Clinical Respiratory Physiology* 2017: 50(2).

26. Mora AL, Rojas M, Pardo A, Selman M. Emerging therapies for idiopathic pulmonary fibrosis, a progressive age-related disease. *Nature reviews Drug discovery* 2017: 16(11): 755-772.

27. Hou F, Sun L, Zheng H, Skaug B, Jiang QX, Chen ZJ. MAVS forms functional prion-like aggregates to activate and propagate antiviral innate immune response. *Cell* 2011: 146(3): 448-461.

28. Sun Q, Sun L, Liu HH, Chen X, Seth RB, Forman J, Chen ZJ. The specific and essential role of MAVS in antiviral innate immune responses. *Immunity* 2006: 24(5): 633-642.

29. Sun X, Sun L, Zhao Y, Li Y, Lin W, Chen D, Sun Q. MAVS maintains mitochondrial homeostasis via autophagy. *Cell discovery* 2016: 2: 16024.

30. Li T, Li X, Attri KS, Liu C, Li L, Herring LE, Asara JM, Lei YL, Singh PK, Gao C, Wen H. O-GlcNAc Transferase Links Glucose Metabolism to MAVS-Mediated Antiviral Innate Immunity. *Cell host & microbe* 2018: 24(6): 791-803 e796.

31. Malsin ES, Kamp DW. The mitochondria in lung fibrosis: friend or foe? *Translational research : the journal of laboratory and clinical medicine* 2018.

32. Matzinger P. The danger model: a renewed sense of self. *Science* 2002: 296(5566): 301-305.

33. Dela Cruz CS, Kang MJ. Mitochondrial dysfunction and damage associated molecular patterns (DAMPs) in chronic inflammatory diseases. *Mitochondrion* 2018: 41: 37-44.

34. Ellson CD, Dunmore R, Hogaboam CM, Sleeman MA, Murray LA. Danger-associated molecular patterns and danger signals in idiopathic pulmonary fibrosis. *American journal of respiratory cell and molecular biology* 2014: 51(2): 163-168.

35. Kang MJ, Yoon CM, Kim BH, Lee CM, Zhou Y, Sauler M, Homer R, Dhamija A, Boffa D, West AP, Shadel GS, Ting JP, Tedrow JR, Kaminski N, Kim WJ, Lee CG, Oh YM, Elias JA. Suppression of NLRX1 in chronic obstructive pulmonary disease. *The Journal of clinical investigation* 2015: 125(6): 2458-2462.

36. Wrighton KH, Lin X, Feng XH. Phospho-control of TGF-beta superfamily signaling. *Cell Res* 2009: 19(1): 8-20.

37. Derynck R, Zhang YE. Smad-dependent and Smad-independent pathways in TGF-beta family signalling. *Nature* 2003: 425(6958): 577-584.

38. Kang MJ. Recent Advances in Molecular Basis of Lung Aging and Its Associated Diseases. *Tuberc Respir Dis (Seoul)* 2020: 83(2): 107-115.

39. Lagares D, Santos A, Grasberger PE, Liu F, Probst CK, Rahimi RA, Sakai N, Kuehl T, Ryan J, Bhola P, Montero J, Kapoor M, Baron M, Varelas X, Tschumperlin DJ, Letai A, Tager

AM. Targeted apoptosis of myofibroblasts with the BH3 mimetic ABT-263 reverses established fibrosis. *Sci Transl Med* 2017: 9(420).

40. Chang J, Wang Y, Shao L, Laberge RM, Demaria M, Campisi J, Janakiraman K, Sharpless NE, Ding S, Feng W, Luo Y, Wang X, Aykin-Burns N, Krager K, Ponnappan U, Hauer-Jensen M, Meng A, Zhou D. Clearance of senescent cells by ABT263 rejuvenates aged hematopoietic stem cells in mice. *Nat Med* 2016: 22(1): 78-83.

41. van Deursen JM. Senolytic therapies for healthy longevity. *Science* 2019: 364(6441): 636-637.

42. Schaefer CJ, Ruhrmund DW, Pan L, Seiwert SD, Kossen K. Antifibrotic activities of pirfenidone in animal models. *European respiratory review : an official journal of the European Respiratory Society* 2011: 20(120): 85-97.

FIGURE 1

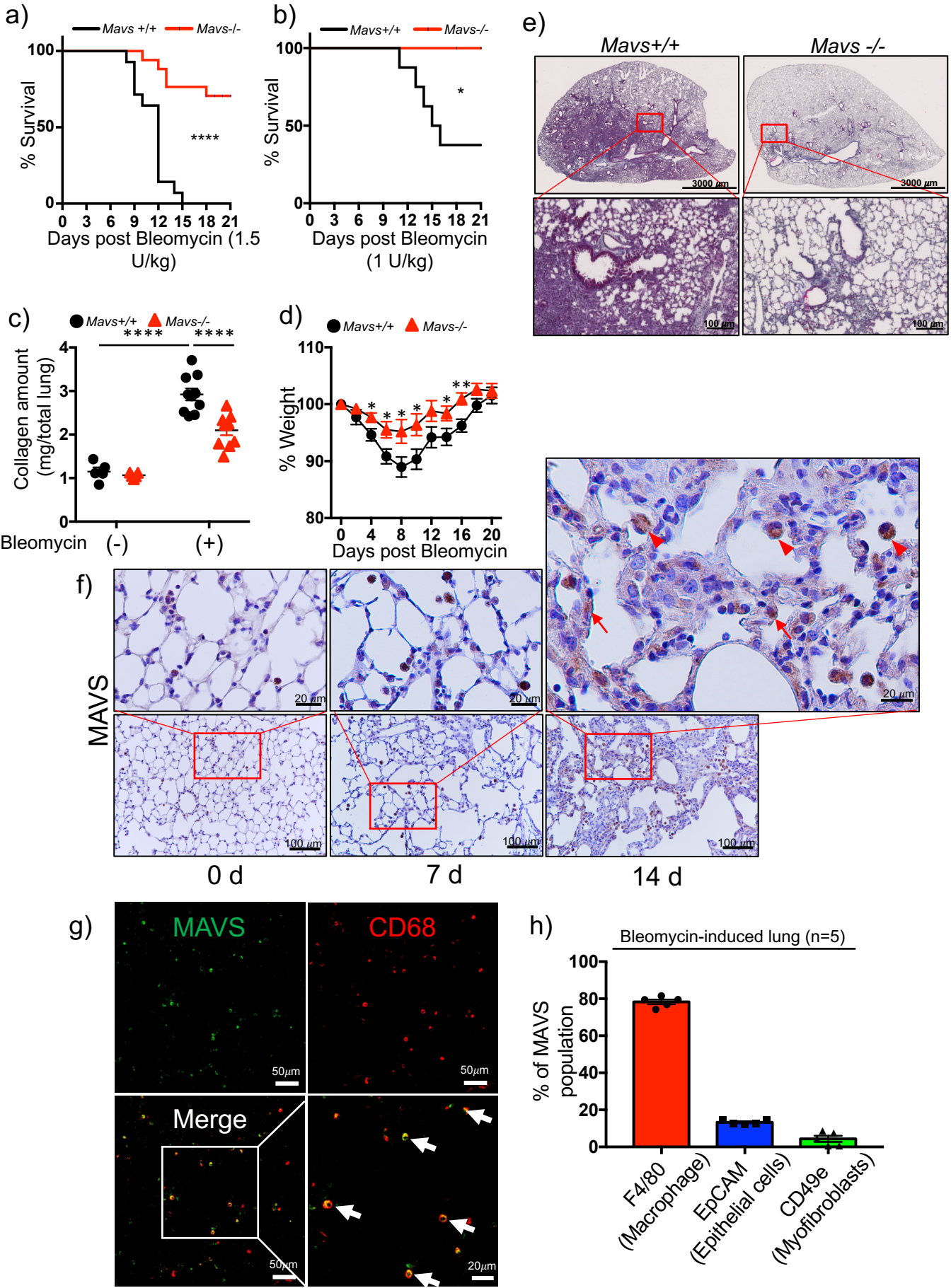
a)
Mavs +/+
Mavs-/-
% Survival
Days post Bleomycin (1.5 U/kg)
****
b)
Mavs+/+
Mavs-/-
% Survival
Days post Bleomycin (1 U/kg)
*
c)
Mavs+/+
Mavs-/-
Collagen amount (mg/total lung)
Bleomycin (-) (+)
d)
Mavs+/+
Mavs-/-
% Weight
Days post Bleomycin
e)
Mavs+/+
Mavs -/-
3000 μm
100 μm
f)
MAVS
20 μm
100 μm
0 d
7 d
14 d
g)
MAVS
CD68
Merge
50μm
20μm
h)
Bleomycin-induced lung (n=5)
% of MAVS population
F4/80 (Macrophage)
EpCAM (Epithelial cells)
CD49e (Myofibroblasts)

Figure 1. MAVS plays a crucial role in lung fibrosis after bleomycin administration *in vivo.*

The indicated dose of bleomycin was administered through intra-tracheal (IT) route to C57BL/6J wild type (*Mavs*+/+) and MAVS null mutant (*Mavs*-/-) mice. (**a** and **b**) Survival rates were monitored during the course of the experiment after (**a**) 1.5 U/kg (n=14 per each of both groups) and (**b**) 1.0 U/kg bleomycin administration (n=8 per *Mavs*+/+, n=7 per *Mavs*-/- group). (**c**-**g**) Saline (bleomycin -) or 0.4 U/kg of bleomycin (+) was administered through IT route to *Mavs*+/+ and *Mavs*-/- mice. (**c**) Collagen contents of total lung tissues obtained from the mice sacrificed at day 21 after bleomycin administration were measured (n=5 per each of both saline groups, n=10 per each of both bleomycin-administered *Mavs*+/+ and *Mavs*-/- mice groups, respectively). (**d**) Body weight changes were monitored during the course of the experiment. (**e**) Representative histologic findings are presented after Masson's trichrome staining of collagen on lung sections at day 21 after bleomycin administration (Scale bars: 3,000 μm (top panels), 100 μm (lower panels)). (**f**) Immunohistochemistry analysis of MAVS on lung sections at indicated time points after saline or bleomycin administration. Representative images of the staining are presented (n=5 per each of the groups). The red boxed regions are magnified for closer observation. Arrows point to alveolar epithelial cells; Arrowheads indicate macrophages. (**g**) Representative images (Scale bars: 50 μm) from the immunofluorescence analysis of MAVS staining (green) on lung sections at 14 d after bleomycin administration are presented (n=5). CD68 antibody (red) was used for the immunofluorescence staining of macrophages. The white boxed region is magnified for closer observation (Scale bars: 20 μm). (h) The percentage of each cell populations among the MAVS-stained lung cells from bleomycin-administered lungs at day 14 was determined by flow cytometry (n=5). Specific surface markers were used to identify lung cell populations; macrophages ($CD45^+F4/80^+$), epithelial cells ($CD45^-CD31^-CD49e^-EpCAM^+$) and myofibroblasts ($CD45^-CD31^-EpCAM^-CD49e^+$). Data are the mean ± SEM. Statistical significance was determined using the log-rank (Mantel-Cox) (**a** and **b**) or 2-way ANOVA with Tukey's multiple comparisons test (**c**) or multiple t test (**d**). *, $P < 0.05$; **, $P < 0.01$; ****, $P < 0.0001$.

FIGURE 2

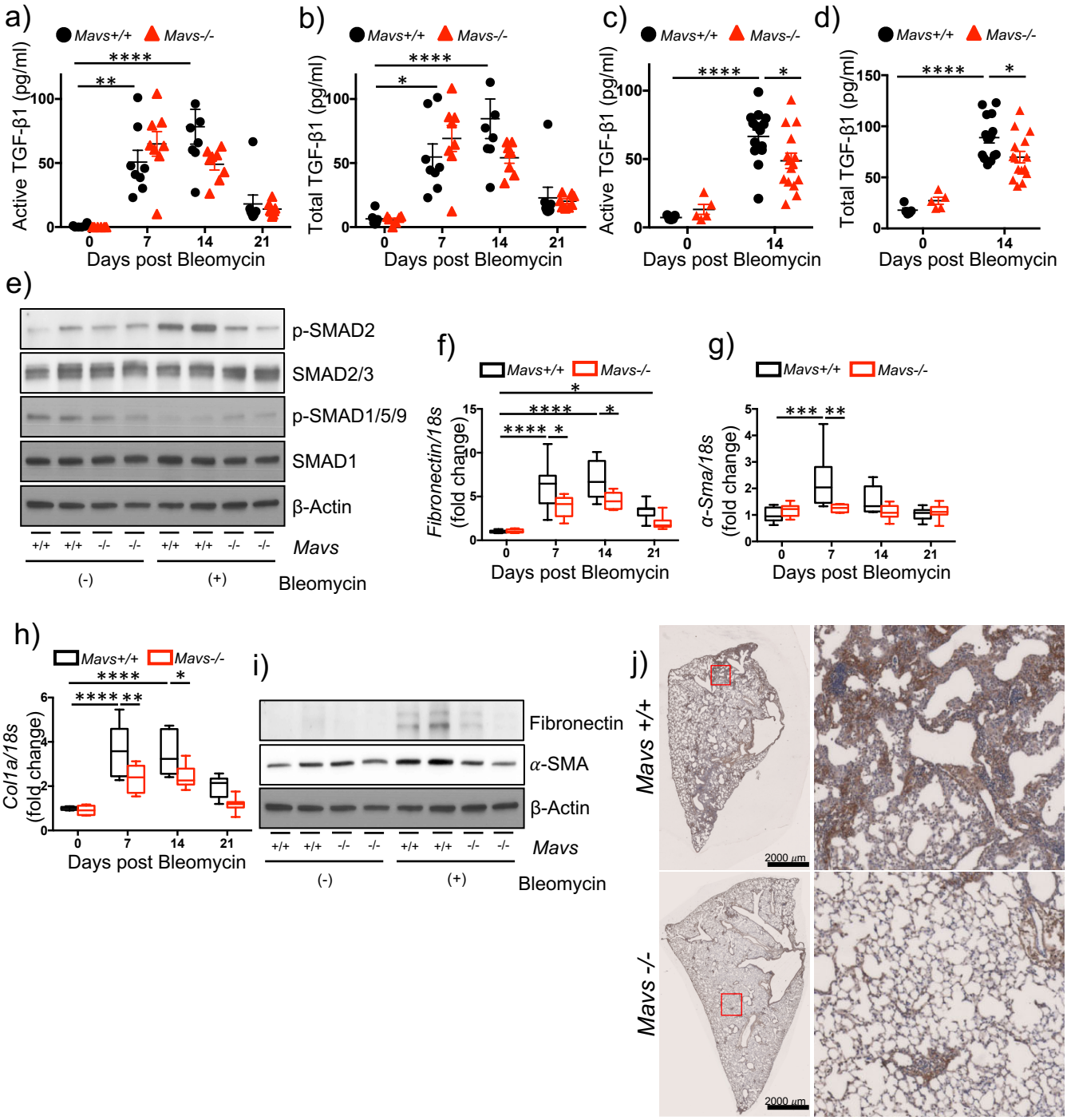
a)
Mavs+/+
Mavs-/-
Active TGF-β1 (pg/ml)
Days post Bleomycin
b)
Total TGF-β1 (pg/ml)
c)
d)
e)
p-SMAD2
SMAD2/3
p-SMAD1/5/9
SMAD1
β-Actin
Mavs
Bleomycin
f)
Fibronectin/18s (fold change)
g)
α-Sma/18s (fold change)
h)
Col1a/18s (fold change)
i)
Fibronectin
α-SMA
β-Actin
j)
Mavs +/+
Mavs -/-
2000 μm

Figure 2. MAVS-dependent and independent fibrogenic responses in bleomycin-induced pulmonary fibrosis

(a-d) Saline (bleomycin -) or bleomycin (+) was administered to wild type (*Mavs*+/+) and MAVS null mutant (*Mavs*-/-) mice. (a) Active and (b) total TGF-β1 levels at indicated time points after bleomycin administration were measured from the bronchoalveolar lavage (BAL) fluid by ELISA (n=6 per saline groups, n=8 per bleomycin-administered groups). (c) Active and (d) total TGF-β1 levels at day 14 after bleomycin administration were measured from the BAL fluid by ELISA. (n=5 per saline groups, n=15 per bleomycin-administered groups). (e) Western blot analysis of p-SMAD2, SMAD2/3, p-SMAD1/5/9, and SMAD1 expressions in whole lung tissue lysates at day 14 after saline or bleomycin administration. β -Actin was used as a loading control. (f-h) qRT-PCR analysis of the expression of (f) *Fibronectin*, (g) Alpha-smooth muscle actin *(α-SMA*) and (h) Collagen 1α (*Col1α*) mRNAs, respectively, in lung tissues at day 14 after saline or bleomycin administration (n=6 per saline group, n=8 per bleomycin-administered group) are illustrated. (i) Western blot analysis of Fibronectin and α-SMA expressions in lung tissue lysates day 14 after saline or bleomycin administration are presented. β-Actin was used as a loading control. (j) Representative images from immunohistochemistry analysis of Col1α on lung sections at day 14 after bleomycin administration are presented (n=5 per each of the groups). Scale bars: 2,000 μm. The red boxed regions are magnified on the right for closer observation. Data are the mean ± SEM or Min to Max. Statistical significance was determined using the 2-way ANOVA with Tukey's multiple comparisons test (a-d and f-h). *, $P < 0.05$; **, $P < 0.01$; ***, $P < 0.001$; ****, $P < 0.0001$.

FIGURE 3

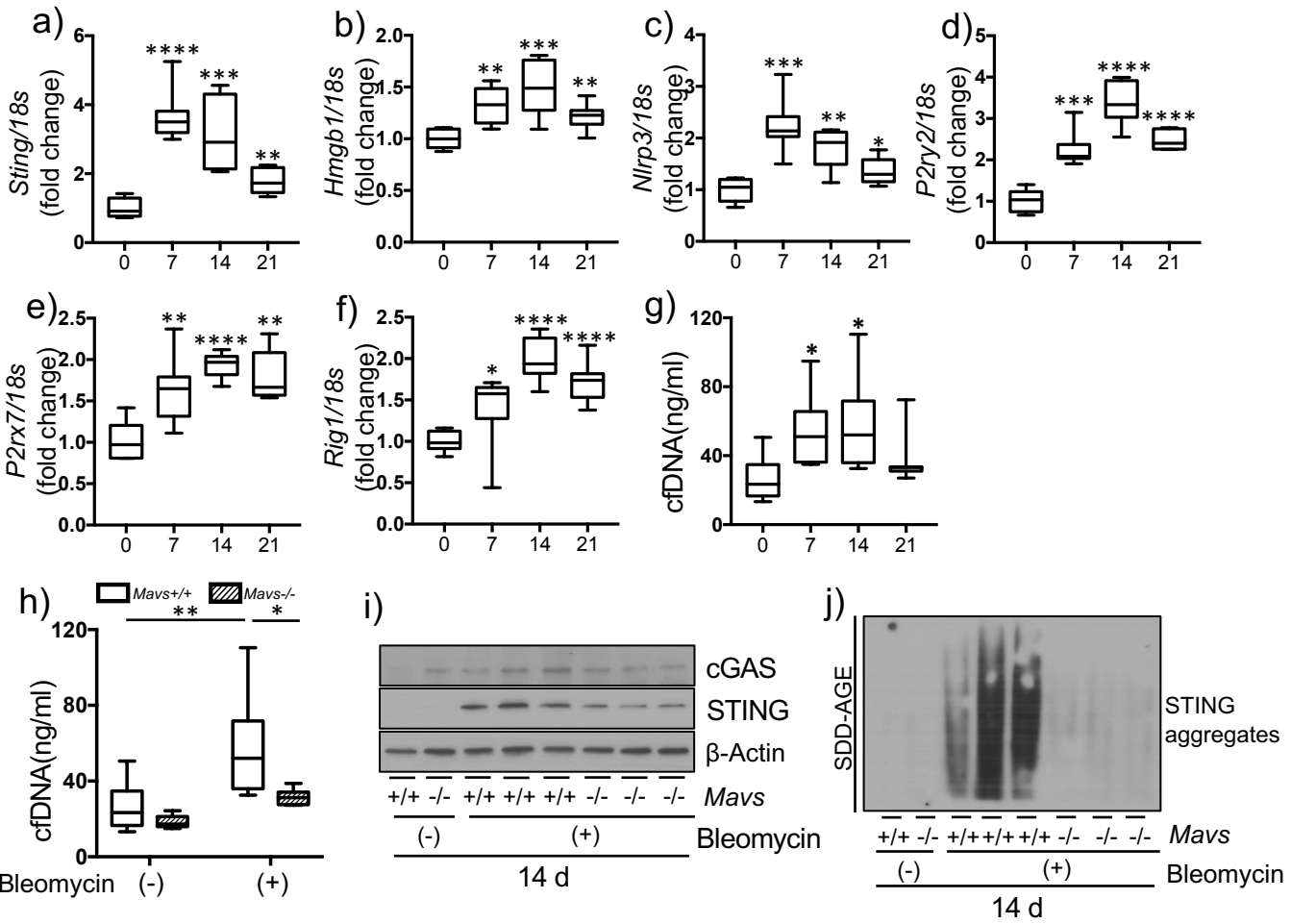
a)
Sting/18s (fold change)
b)
Hmgb1/18s (fold change)
c)
Nlrp3/18s (fold change)
d)
P2ry2/18s (fold change)
e)
P2rx7/18s (fold change)
f)
Rig1/18s (fold change)
g)
cfDNA(ng/ml)
0 7 14 21
h)
Mavs+/+
Mavs-/-
cfDNA(ng/ml)
Bleomycin (-) (+)
i)
cGAS
STING
β-Actin
+/+ -/- +/+ +/+ +/+ -/- -/- -/-
Mavs
(-) (+)
Bleomycin
14 d
j)
SDD-AGE
STING aggregates
+/+ -/- +/+ +/+ +/+ -/- -/- -/-
Mavs
(-) (+)
Bleomycin
14 d

Figure 3. MAVS amplifies multiple DAMPs signaling during fibrotic phase.

(a-g) Saline (bleomycin -) or bleomycin (+) was administered to wild type mice. (a-f) From whole lung tissues at the indicated time points after bleomycin administration, the expression levels of (a) *Sting*, (b) *Hmgb1*, (c) *Nlrp3*, (d) *P2ry2*, (eE) *P2rx7*, and (f) *Rig-I* mRNAs, respectively, were evaluated by qRT-PCR. (g) The amount of cell-free dsDNA (cfDNA) in BAL fluid was evaluated by fluorometric assay. (h-j) Saline (bleomycin -) or bleomycin (+) was administered to wild type (*Mavs*+/+) and MAVS null mutant (*Mavs*-/-) mice. (h) The results of cfDNA amount from BAL fluid, and (i) Western blot evaluations for cGAS and STING proteins from whole lung tissue lysates, respectively, at day 14 after bleomycin administration are presented. β-Actin was used as a loading control. (j) The result of STING aggregation is presented. Lung tissue lysates at day 14 after bleomycin administration were separated by semi-denaturating detergent agarose gel electrophoresis (SDD-AGE) and detected with STING antibody. Data are the mean Min to Max. Statistical significance was determined using unpaired t test (a-g) or 2-way ANOVA with Tukey's multiple comparisons test (h). *, $P < 0.05$; **, $P < 0.01$; ***, $P < 0.001$; ****, $P < 0.0001$.

FIGURE 4

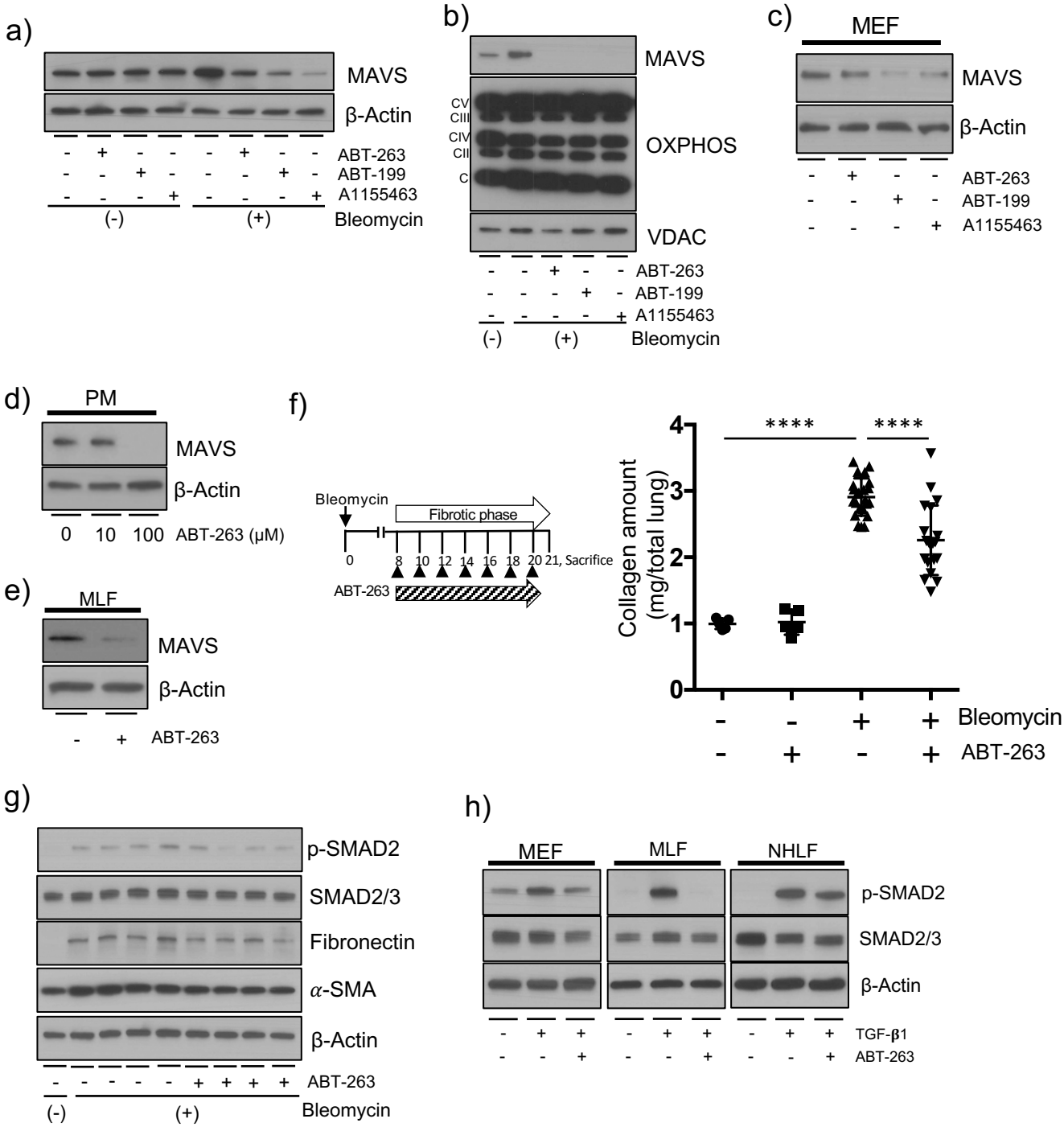
a)
MAVS
β-Actin
ABT-263
ABT-199
A1155463
(-)
(+)
Bleomycin
b)
MAVS
CV
CIII
CIV
CII
C
OXPHOS
VDAC
ABT-263
ABT-199
A1155463
(-)
(+)
Bleomycin
c)
MEF
MAVS
β-Actin
ABT-263
ABT-199
A1155463
d)
PM
MAVS
β-Actin
0
10
100
ABT-263 (μM)
e)
MLF
MAVS
β-Actin
ABT-263
f)
Bleomycin
Fibrotic phase
0
8
10
12
14
16
18
20
21, Sacrifice
ABT-263
Collagen amount (mg/total lung)
****
****
Bleomycin
ABT-263
g)
p-SMAD2
SMAD2/3
Fibronectin
α-SMA
β-Actin
ABT-263
(-)
(+)
Bleomycin
h)
MEF
MLF
NHLF
p-SMAD2
SMAD2/3
β-Actin
TGF-β1
ABT-263

Figure 4. A BH3 mimetic ABT-263 attenuates the expression of MAVS and lung fibrosis.

(a-e) The indicated BH3 mimetics with 100 μM amounts, respectively, were treated for 3 h. (a) MLE-12 cells were treated with the indicated BH3 mimetics after 10 mU/ml bleomycin treatment for 3 days. The expression of MAVS was evaluated by Western blot analysis. (b) The mitochondrial fractions of MLE-12 cells treated with the indicated BH3 mimetics after 10 mU/ml bleomycin treatment for 3 days, respectively. The expression of MAVS and Oxidative phosphorylation (OXPHOS) complexes were evaluated by Western blot analysis. Voltage-dependent anionic channel (VDAC) protein was evaluated as loading controls of mitochondria. (c) The mouse embryonic fibroblasts (MEF) cells were treated with the indicated BH3 mimetics. The expression of MAVS was evaluated by Western blot analysis. (d) Primary peritoneal macrophages (PM) were isolated from the peritoneal cavity of wild type mice. The cells were treated with 10 and 100 μM ABT-263. The expression of MAVS was evaluated by Western blot analysis. (e) Primary murine lung fibroblasts (MLF) were isolated from wild type murine lungs. The cells were treated with ABT-263. The expression of MAVS was evaluated by Western blot analysis. (f) The Scheme of the experimental approach, and evaluation results of the total lung collagen contents from wild type murine lungs are presented. The mice were administered with bleomycin (+) and treated after day 8 with ABT-263 (40 mg/kg, every 2 d, i.p.), and sacrificed at day 21. Each dot indicates the individual mouse used for the experiment. (n=5 per each of both control groups, n=23 per bleomycin only treatment group, n=20 per bleomycin+ABT-263 treatment group, respectively). (g) Western blot evaluations for p-SAMD2, SMAD2/3, Fibronectin and a-SMA proteins from whole lung tissue lysates, respectively, at day 14 after bleomycin administration are presented. (n=5 per each of the groups). (h) After stimulation with 20 ng/ml TGF-β1 for 24 h, MEF, MLF and human normal lung fibroblasts (NHLF) were treated with 100 μM ABT-263 for 3 h. Then, the expression of p-SMAD2, SMAD2/3, respectively, were evaluated by Western blot analysis. For panels (a), (c-e) and (g-h), β-Actin was used as a loading control. Data are the mean ± SEM. Statistical significance was calculated using the 2-way ANOVA with Tukey's multiple comparisons test (f) ****, $P < 0.0001$.

FIGURE 5

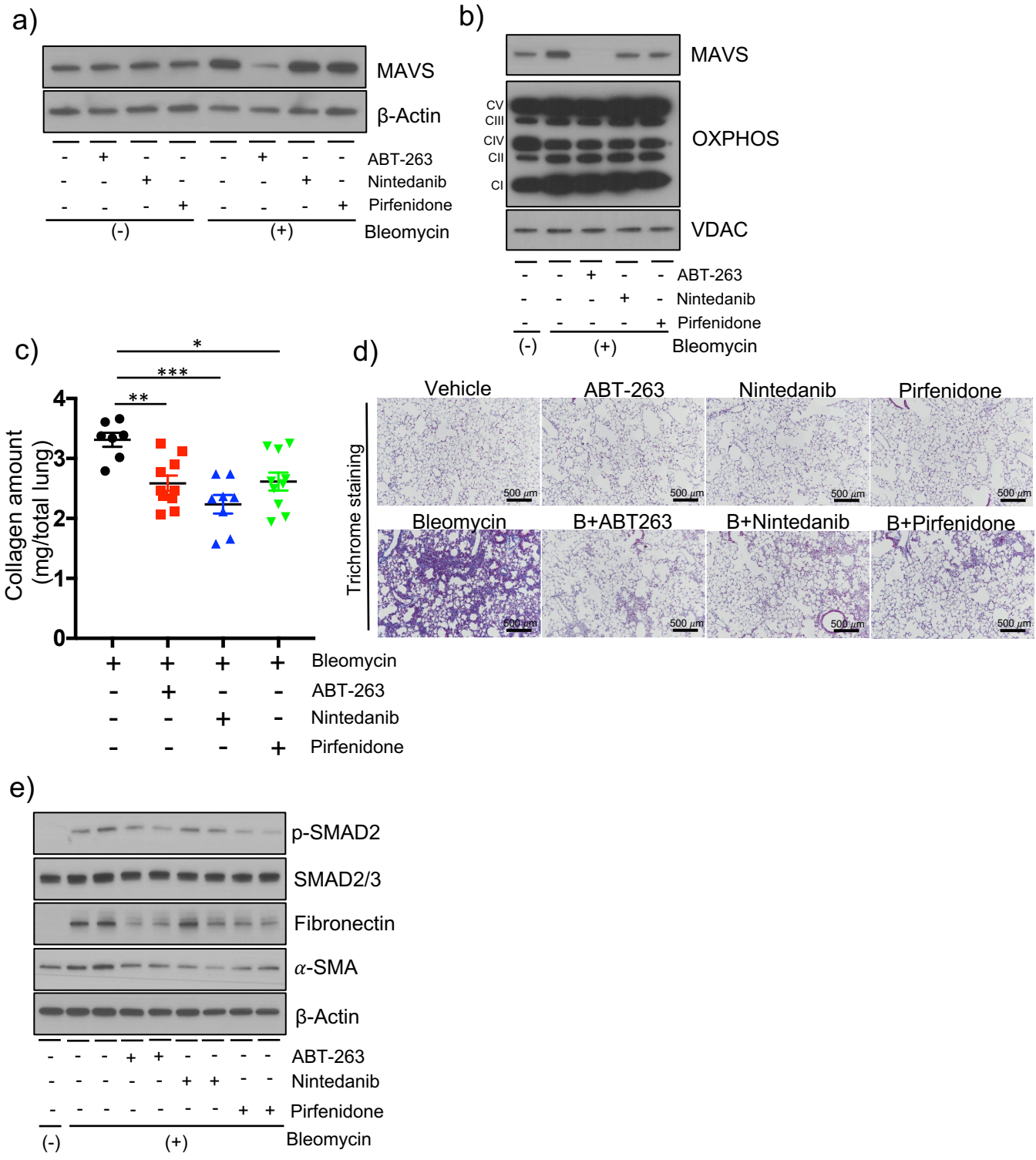
a)
MAVS
β-Actin
ABT-263
Nintedanib
Pirfenidone
(-)
(+)
Bleomycin
b)
MAVS
CV
CIII
CIV
CII
CI
OXPHOS
VDAC
ABT-263
Nintedanib
Pirfenidone
(-)
(+)
Bleomycin
c)
Collagen amount (mg/total lung)
*
***
**
Bleomycin
ABT-263
Nintedanib
Pirfenidone
d)
Vehicle
ABT-263
Nintedanib
Pirfenidone
Trichrome staining
Bleomycin
B+ABT263
B+Nintedanib
B+Pirfenidone
500 μm
e)
p-SMAD2
SMAD2/3
Fibronectin
α-SMA
β-Actin
ABT-263
Nintedanib
Pirfenidone
(-)
(+)
Bleomycin

Figure 5. Therapeutic effects of Nintedanib or Pirfenidone, two approved drugs, are not related to MAVS.

(a-b) MLE-12 cells were treated with ABT-263 (100 μM), Nintedanib (100 μM) and Pirfenidone (100 μM) for 3 h after 10 mU/ml bleomycin treatment for 3 days. The expression of MAVS from (a) whole cell lysates, and (b) mitochondrial fractions, respectively, was evaluated by Western blot analysis. In panel (b), the expression of OXPHOS complexes and VDAC protein as loading controls of mitochondria are presented. (c) The evaluation results of the total lung collagen contents and (d) the representative images of Masson's trichrome staining evaluation are presented. C57BL/6J wild type mice were administered with bleomycin (+) and treated after day 8 with ABT-263 (40 mg/kg, every 2 d, i.p.), Nintedanib (40 mg/kg, every 2 d, i.p.) and Pirfenidone (40 mg/kg, every 2 d, i.p.), and sacrificed at day 21. Each dot indicates the individual mouse used for the experiment. (n=10 per bleomycin treatment group (3-mice dead), n=10 per Bleomycin+ABT-263 treatment group, n=10 per Bleomycin+Nintedanib treatment group (2-mice dead) and n=10 per Bleomycin+Pirfenidone treatment group, respectively). (Scale bars: 500 μm). (e) Western blot evaluations for p-SAMD2, SMAD2/3, Fibronectin and a-SMA proteins from whole lung tissue lysates, respectively, at day 14 after bleomycin administration are presented. For panels (a) and (e), β-Actin was used as a loading control. Data are the mean ± SEM. Statistical significance was calculated using the 2-way ANOVA with Tukey's multiple comparisons test (c) *, $P < 0.05$; **, $P < 0.01$; ***, $P < 0.001$.

FIGURE 6

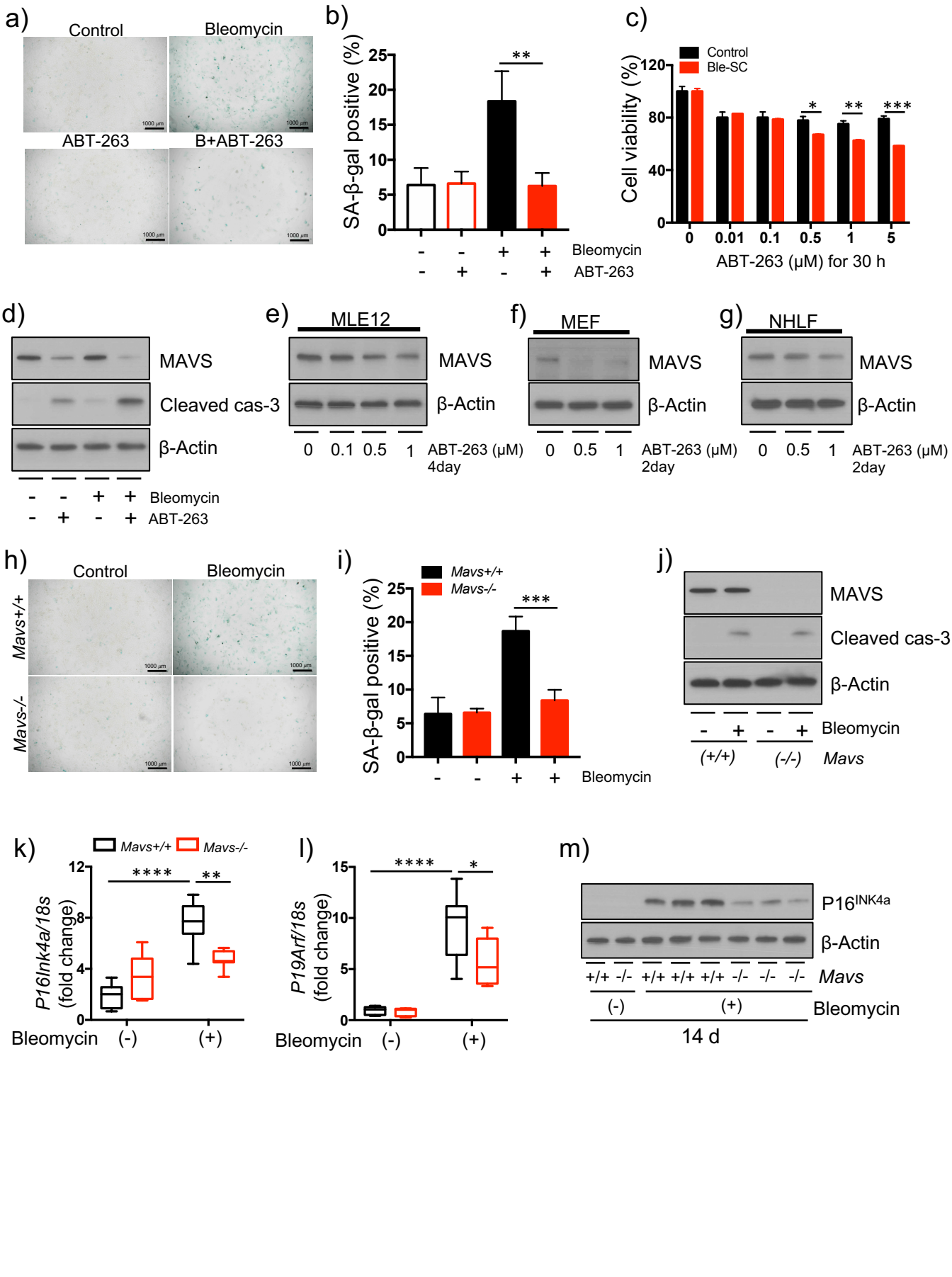
a)
Control
Bleomycin
ABT-263
B+ABT-263
b)
SA-β-gal positive (%)
Bleomycin
ABT-263
c)
Control
Ble-SC
Cell viability (%)
ABT-263 (μM) for 30 h
d)
MAVS
Cleaved cas-3
β-Actin
Bleomycin
ABT-263
e)
MLE12
ABT-263 (μM) 4day
f)
MEF
ABT-263 (μM) 2day
g)
NHLF
ABT-263 (μM) 2day
h)
Control
Bleomycin
Mavs+/+
Mavs-/-
i)
Mavs+/+
Mavs-/-
SA-β-gal positive (%)
Bleomycin
j)
MAVS
Cleaved cas-3
β-Actin
Bleomycin
Mavs
k)
Mavs+/+
Mavs-/-
P16Ink4a/18s (fold change)
Bleomycin
l)
P19Arf/18s (fold change)
Bleomycin
m)
P16INK4a
β-Actin
Mavs
Bleomycin
14 d

Figure 6. Bleomycin-induced cellular senescence is inhibited in MAVS deficiency.

(a-d) MEF cells were treated with indicated concentration of ABT-263 for 30 h after 50 mU/ml bleomycin treatment. (a) The result of SA-β-Gal staining and (b) quantification of SA-β-gal-positive cells are presented (Scale bars: 100 μm). (c) Cell viability was measured by XTT assay. (d) The Western blot results of MAVS and Cleaved caspase-3 (cas-3) proteins are presented. (e) MLE-12, (f) MEF and (g) NHLF cells were treated with the indicated concentration of ABT-263 for indicated time points, respectively. The expression of MAVS was evaluated by Western blot analysis. (h-i) *Mavs*+/+ and *Mavs*-/- MEF cells were treated with 1 μM ABT-263 for 30 h after 50 mU/ml bleomycin treatment. (h) The result of SA-β-Gal staining and (i) quantification of SA-β-gal-positive cells are presented (Scale bars: 100 μm). (j) *Mavs*+/+ and *Mavs*-/- MEF cells were treated with 50 mU/ml bleomycin treatment for 30 h. The Western blot results of MAVS and Cleaved caspase-3 (cas-3) proteins are presented. (k-m) Saline (bleomycin -) or bleomycin (+) was administered to wild type (*Mavs*+/+) and MAVS null mutant (*Mavs*-/-) mice. From whole lung tissues at day 14 after bleomycin administration, the expression levels of (k) $P16^{INK4a}$ and (l) $P19^{ARF}$ were evaluated by qRT-PCR, respectively. (m) The Western blot result of $P16^{INK4a}$ protein is presented. For panels (d), (e), (f), (g) (j) and (m), β-Actin was used as a loading control. Data are the mean ± SD. Statistical significance was calculated using the 2-way ANOVA with Tukey's multiple comparisons test *, $P < 0.05$; **, $P < 0.01$; ***, $P < 0.001$.

FIGURE 7

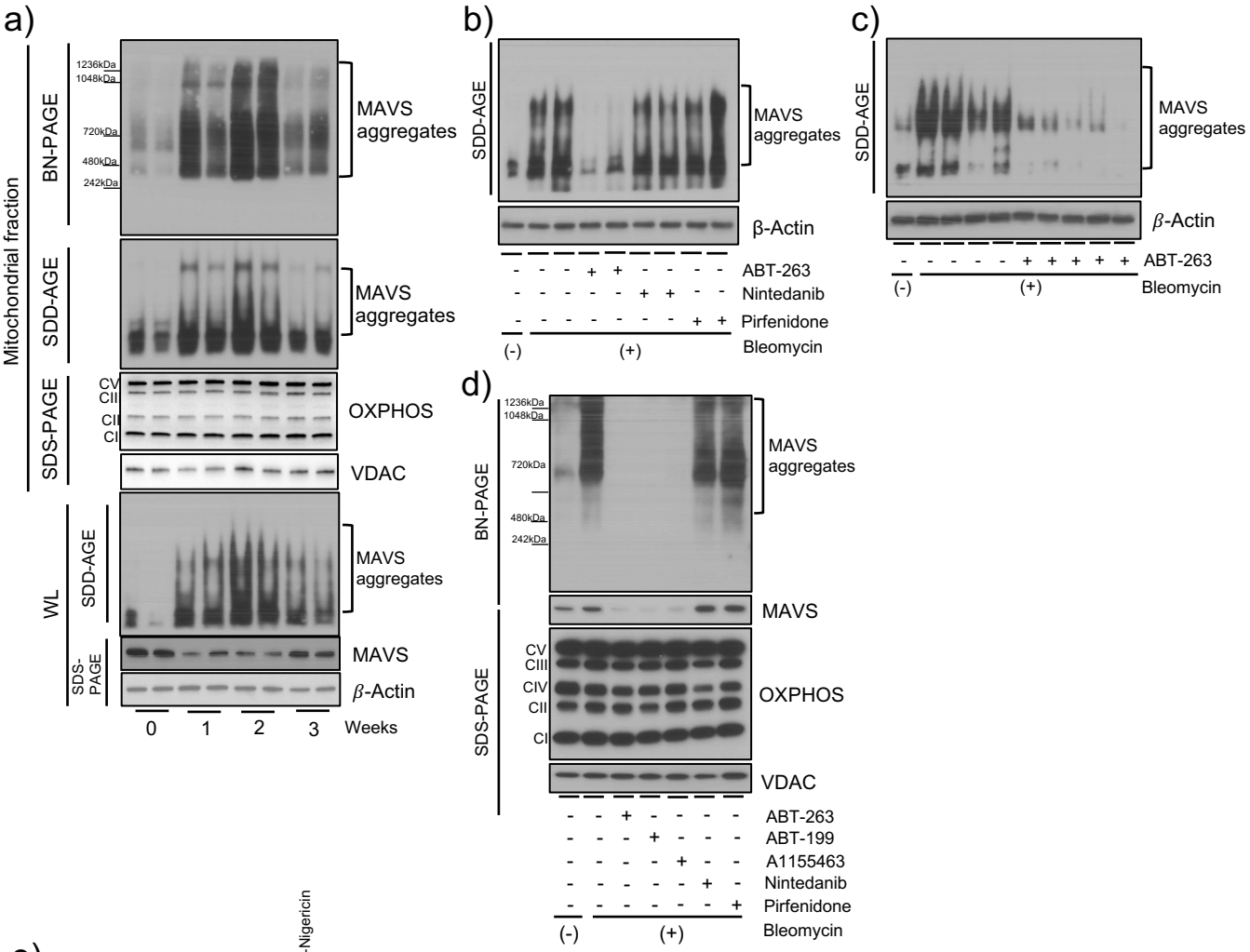

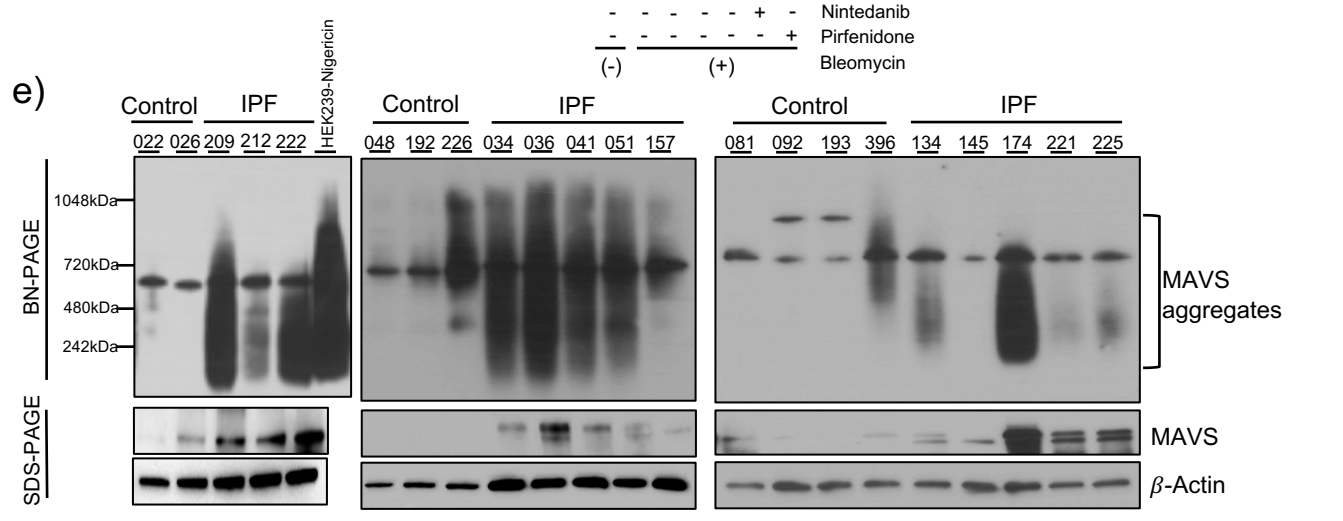

f)

	MAVS aggregate	
	NO	Yes
Control	7	2
IPF	2	11

Fisher's exact test
****, *P* = 0.0073**

Figure 7. Multimeric aggregation of MAVS, a critical event of MAVS signaling, is significantly activated in humans as well as in mice

(a) Saline (bleomycin -) or bleomycin (+) was administered to wild type (*Mavs*+/+) mice. The multimeric MAVS aggregation from whole lung tissue lysates (WL) and mitochondrial fractions (MF) at indicated time points was evaluated by blue native (BN)-PAGE and SDD-AGE. (b-c) Wild type mice were administered with bleomycin (+) and treated after day 8 with ABT-263 (40 mg/kg, every 2 d, i.p.), Nintedanib (40 mg/kg, every 2 d, i.p.) and Pirfenidone (40 mg/kg, every 2 d, i.p.). The multimeric MAVS aggregation in WL at day 14 was evaluated by SDD-AGE. (d) The mitochondrial fractions of MLE-12 cells treated with 100 μM ABT-263, ABT-199, A-1155463, Nintedanib and Pirfenidone, respectively, for 3 h after 10 mU/ml bleomycin treatment for 3 days. The multimeric MAVS aggregation and expression of MAVS and OXPHOS complexes were evaluated by BN-PAGE and SDS-PAGE, respectively. VDAC protein was evaluated as loading controls of mitochondria for panels (a) and (e). (e) The multimeric MAVS aggregation was evaluated and compared by the application of BN-PAGE from lungs obtained from the patients with IPF or healthy controls. (n=9 per normal group, n=13 per IPF group; each number indicates an individual subject). The cell lysate from human embryonic kidney 293 cells treated with nigericin was used as a positive control in order to evaluate MAVS aggregation. β-Actin was used as a loading control for panels (a), (b), (c) and (e). (f) Fisher's exact test was applied to determine statistical significance of the above result presented in panel D. **, $P < 0.01$.

Supplementary Information

Supplementary Figures and Figure Legends

Figure S1

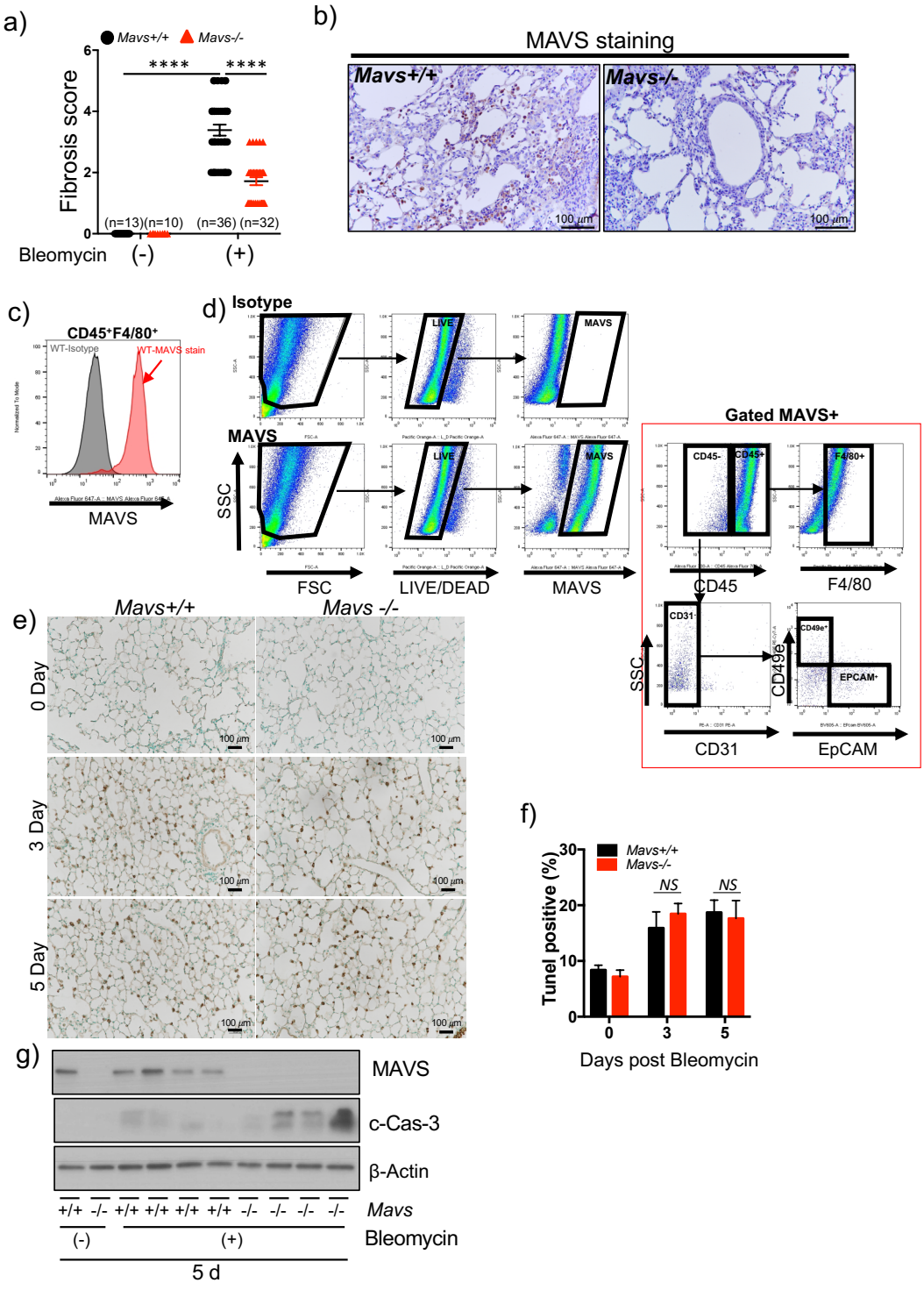

Figure S1 (related to Figure 1). MAVS plays a crucial role in lung fibrosis after bleomycin administration in vivo:

(a) Semi-quantitative evaluation of tissue fibrosis score is presented from lung sections at day 21 after saline (n=13 per *Mavs*+/+, n=10 per *Mavs*-/- group) and bleomycin administration (n=36 per *Mavs*+/+, n=32 per *Mavs*-/- group). (b) Immunohistochemistry evaluations were undertaken to localize the expression of MAVS protein in the lung tissue sections obtained from the mice sacrificed at day 14 after bleomycin administration. Representative images (n=5 per each group) are presented (Scale bars: 100 μm). The lung tissue section from *Mavs-/-* mice was used as a negative control for the evaluation of MAVS staining.

(c) The Expression of MAVS on macrophage ($CD45^+F4/80^+$) population from bleomycin administered lung. The fluorescence intensity of Alexa fluor 647-MAVS (red) or Alexa fluor 647-conjugated isotype control (gray) is shown. (d) The Gating strategy to identify the percentage of each cell population among the MAVS-stained lung cells after bleomycin administration. As a control, Alexa fluor 647-conjugated isotype control antibody was used. (e-g) Saline (bleomycin -) or bleomycin (+) was administered to wild type (*Mavs*+/+) and MAVS null mutant (*Mavs-/-*) mice. (e) Representative images (Scale bars: 100 μm) of TUNEL assay and (f) quantitative results of the percentage of TUNEL-positive cells are presented from the lung sections at indicated time points after bleomycin administration (n=5 per each of the groups). (g) Western blot results of MAVS and Cleaved capase-3 proteins from whole lung tissue lysates at day 5 after bleomycin administration are presented. β-Actin was used as a loading control. Data are the mean ± SEM. Statistical significance was determined using the 2-way ANOVA with Tukey's multiple comparisons test (a and f). ****, $P < 0.0001$.

Figure S2

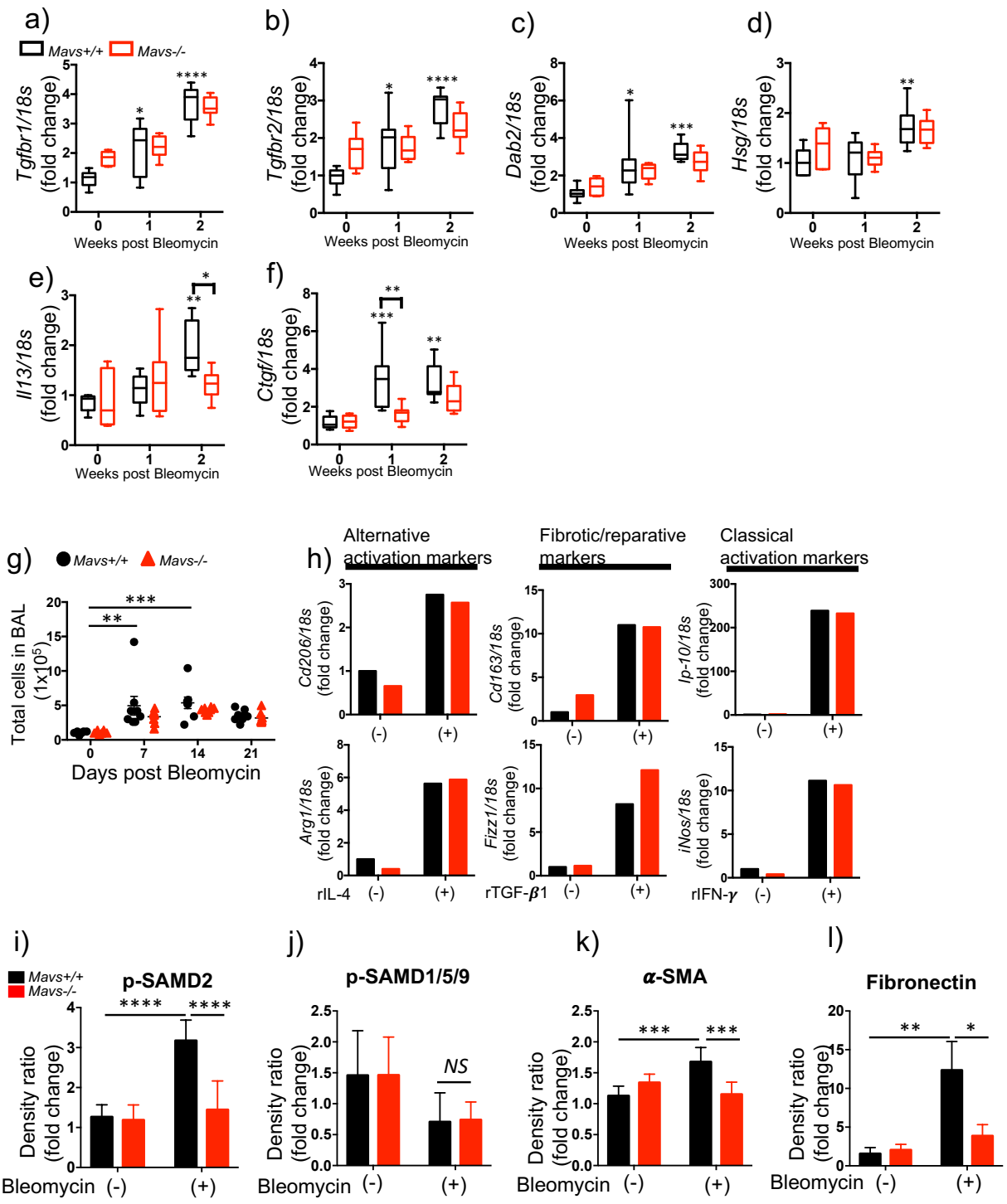
a)
Mavs+/+
Mavs-/-
Tgfbr1/18s (fold change)
Weeks post Bleomycin
b)
Tgfbr2/18s (fold change)
Weeks post Bleomycin
c)
Dab2/18s (fold change)
Weeks post Bleomycin
d)
Hsg/18s (fold change)
Weeks post Bleomycin
e)
Il13/18s (fold change)
Weeks post Bleomycin
f)
Ctgf/18s (fold change)
Weeks post Bleomycin
g)
Mavs+/+
Mavs-/-
Total cells in BAL (1x10^5)
Days post Bleomycin
h)
Alternative activation markers
Fibrotic/reparative markers
Classical activation markers
Cd206/18s (fold change)
Cd163/18s (fold change)
Ip-10/18s (fold change)
Arg1/18s (fold change)
Fizz1/18s (fold change)
iNos/18s (fold change)
rIL-4
rTGF-β1
rIFN-γ
i)
Mavs+/+
Mavs-/-
p-SAMD2
Density ratio (fold change)
Bleomycin
j)
p-SAMD1/5/9
NS
k)
α-SMA
l)
Fibronectin

Figure S2 (related to Figure 2). MAVS-dependent and independent fibrogenic responses in bleomycin-induced pulmonary fibrosis

(a-f) Saline (bleomycin -) or bleomycin (+) was administered to wild type (*Mavs+/+*) and MAVS null mutant (*Mavs-/-*) mice. From whole lung tissues at the indicated time points after bleomycin administration, the expression levels of (a) Transforming growth factor beta receptor 1 (*Tgfbr1)*, (b) Transforming Growth factor beta receptor 2 (*Tgfbr2)*, (c) Disabled homolog 2 (*Dab2)*, (d) Hepatocyte growth factor-regulated tyrosine kinase substrate (*Hsg)*, (e) Interleukin 13 (*Il13)*, and (f) Connective tissue growth factor (*Ctgf*) mRNAs, respectively, were evaluated by qRT-PCR. (g) Total cell counts of the BAL fluid (n=6 per saline group, n=8 per bleomycin administration group) were evaluated. (h) Alveolar macrophages were isolated and pooled from *Mavs+/+* (n = 5) or *Mavs-/-* mice (n = 5), respectively, and stimulated with recombinant IL-4 (20 ng/ml, for alternative activation markers), TGF-β1 (20 ng/ml, for fibrotic/reparative markers) and IFN-γ (100 ng/ml, for classical activation markers) for 18 h. Then, qRT-PCR analysis of the expression of *Cd206, Arg1, Cd163, Fizz1, Ip-10,* and *iNos* mRNAs, respectively, were undertaken. (i-l) The densitometric quantification of (g) p-SMAD2, (h) p-SMAD1/5/9, (i) α-SMA, and (j) Fibronectin, respectively, were evaluated. Values of p-SMAD2 and p-SMAD1/5/9 were normalized against total SMAD2/3 and SMAD1, respectively. Values of α-SMA and Fibronectin were normalized against β-Actin. Data are the mean ± SEM (a-g) or SD (i-l). Statistical significance was determined using the 2-way ANOVA with Tukey's multiple comparisons test (a-l). *, $P < 0.05$; **, $P < 0.01$; ***, $P < 0.001$; ****, $P < 0.0001$.

Figure S3

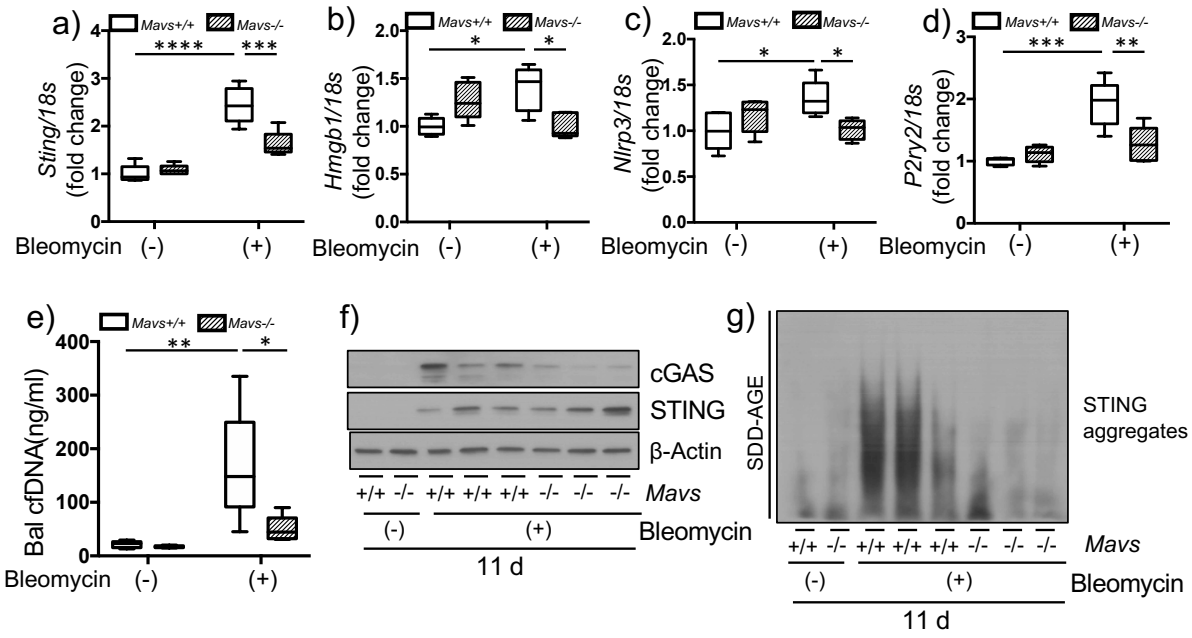
a)
Mavs+/+
Mavs-/-
****
***
Sting/18s (fold change)
Bleomycin (-) (+)
b)
*
*
Hmgb1/18s (fold change)
c)
Nlrp3/18s (fold change)
d)
***
**
P2ry2/18s (fold change)
e)
**
*
Bal cfDNA(ng/ml)
f)
cGAS
STING
β-Actin
+/+ -/- +/+ +/+ +/+ -/- -/- -/-
Mavs
(-) (+)
Bleomycin
11 d
g)
SDD-AGE
STING aggregates
+/+ -/- +/+ +/+ +/+ -/- -/- -/-
Mavs
(-) (+)
Bleomycin
11 d

Figure S3 (related to Figure 3). MAVS amplifies multiple DAMPs signaling during fibrotic phase

(a-g) Saline (bleomycin -) or 1.0 U/kg of bleomycin (+) was administered through IT route to Mavs+/+ and Mavs-/- mice and sacrificed at day 11 time point. From whole lung tissues, the expression levels of (a) *Sting*, (b) *Hmgb1*, (c) *Nlrp3*, and (d) *P2ry2* mRNAs, respectively, were evaluated by qRT-PCR. (e) The amount of cell-free dsDNA (cfDNA) in BAL fluid were evaluated by fluorometric assay (f) The Western blot results of cGAS and STING proteins from whole lung tissue lysates are presented. β-Actin was used as a loading control. (g) The result of STING aggregation by semi-denaturating detergent agarose gel electrophoresis (SDD-AGE) is presented. Data are the mean Min to Max. Statistical significance was determined using 2-way ANOVA with Tukey's multiple comparisons test (a-e). *, $P < 0.05$; **, $P < 0.01$; ***, $P < 0.001$; ****, $P < 0.0001$.

Figure S4

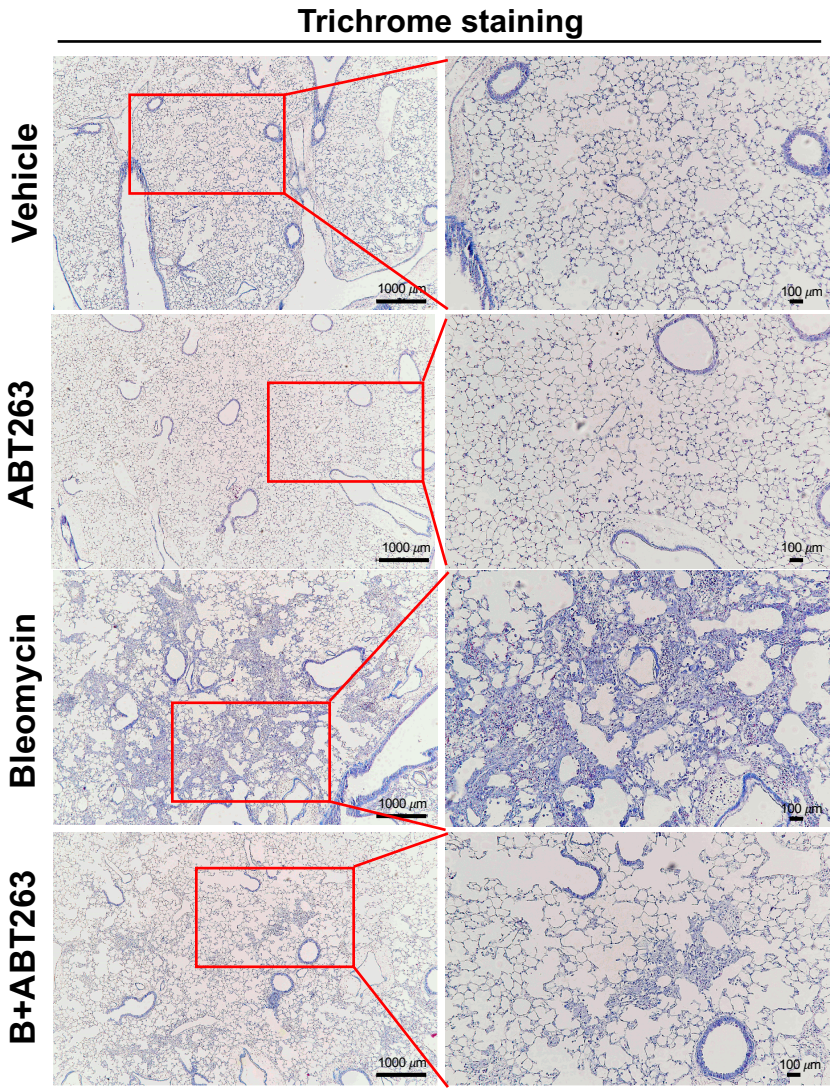
Trichrome staining
Vehicle
ABT263
Bleomycin
B+ABT263
1000 μm
100 μm

Figure S4 (related to Figure 4). A BH3 mimetic ABT-263 attenuates the expression of MAVS and lung fibrosis

The evaluation results of Masson's trichrome staining are presented from the C57BL/6J wild type mice which were administered with 0.4U/kg of bleomycin (+) and treated after day 8 with ABT-263 (40 mg/kg, every 2 d, i.p.) (Scale bars: 1,000 μm (left panels), 100 μm (right panels)). Representative images of the staining are presented (n=5 per each of the groups).

Figure S5

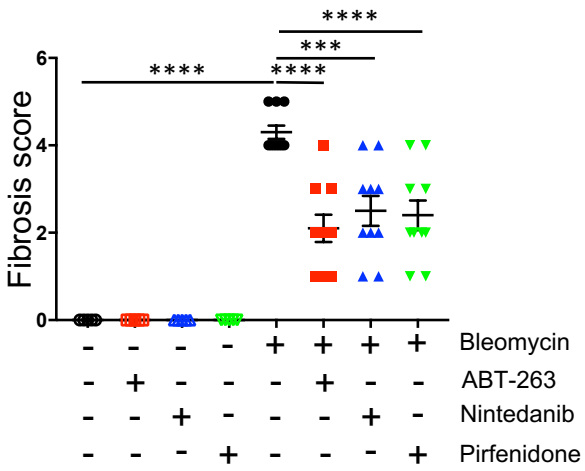
****
***
****
****
Fibrosis score
6
4
2
0
- - - - + + + + Bleomycin
- + - - - + - - ABT-263
- - + - - - + - Nintedanib
- - - + - - - + Pirfenidone

Figure S5 (related to Figure 5). Therapeutic effects of Nintedanib or Pirfenidone, two approved drugs, are not related to MAVS.

Semi-quantitative evaluation of tissue fibrosis score is presented from the lung sections at day 21 after saline (n=5 per each group) or bleomycin administration (n=10 per each group). Data are the mean ± SEM. Statistical significance was determined using the 2-way ANOVA with Tukey's multiple comparisons test. ***, $P < 0.001$; ****, $P < 0.0001$.

Figure S6

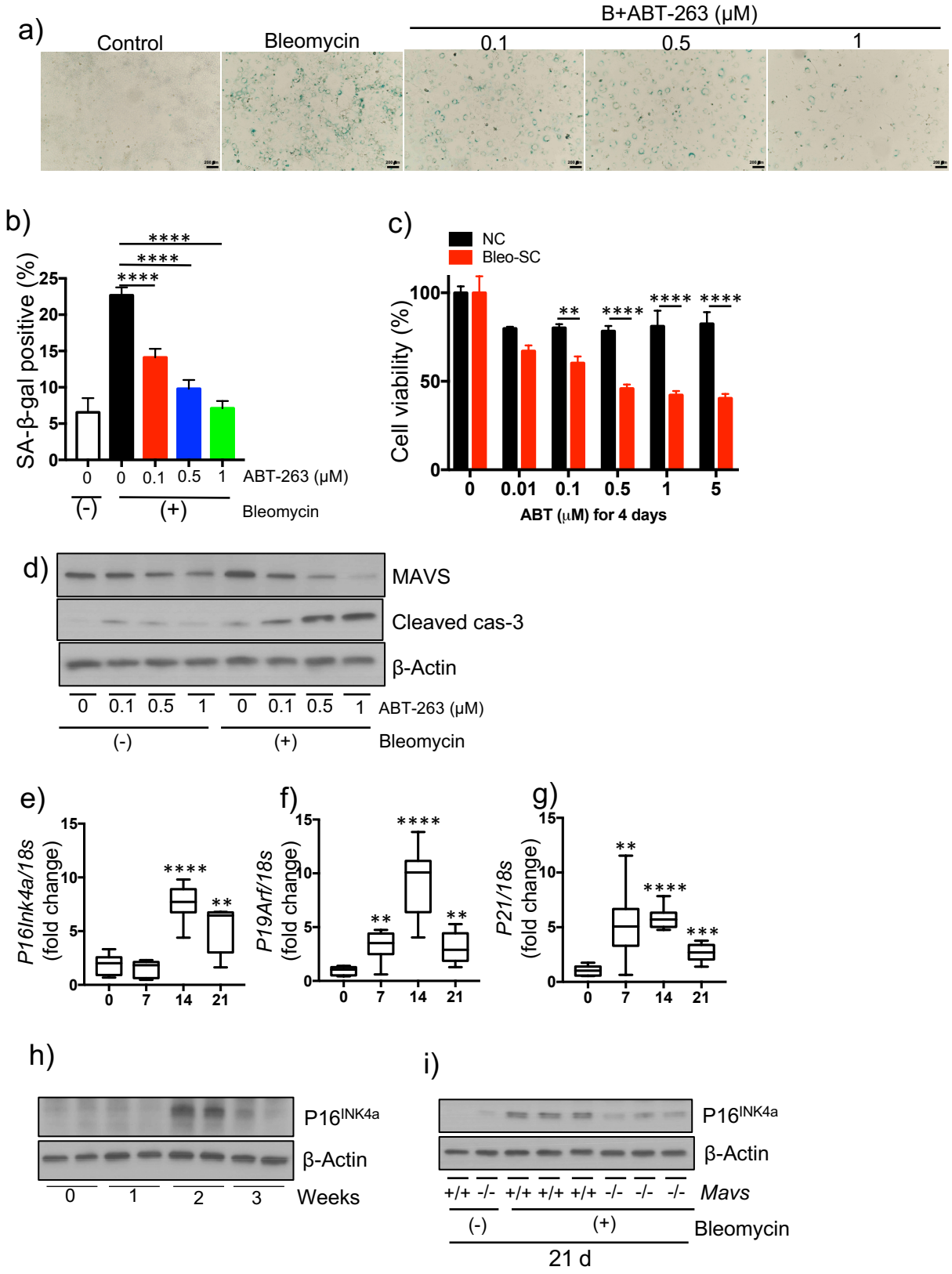
a)
Control
Bleomycin
B+ABT-263 (μM)
0.1
0.5
1
b)
SA-β-gal positive (%)
ABT-263 (μM)
Bleomycin
(-)
(+)
c)
NC
Bleo-SC
Cell viability (%)
ABT (μM) for 4 days
d)
MAVS
Cleaved cas-3
β-Actin
ABT-263 (μM)
Bleomycin
e)
P16Ink4a/18s (fold change)
f)
P19Arf/18s (fold change)
g)
P21/18s (fold change)
h)
P16INK4a
β-Actin
Weeks
i)
P16INK4a
β-Actin
Mavs
Bleomycin
21 d

Figure S6 (related to Figure 6). Bleomycin-induced cellular senescence is inhibited in MAVS deficiency.

(a-d) MLE-12 cells were treated with the indicated concentration of ABT-263 for 4 days after stimulation with vehicle (bleomycin -) or 10 mU/ml of bleomycin (+), respectively. (a)The result of SA-β-Gal staining and (b) the quantification result of SA-β-gal-positive cells are presented (Scale bars: 200 μm). (c) Cell viability was measured by XTT assay. (d) Western blot results of MAVS and Cleaved caspase-3 (cas-3) proteins are presented. β-Actin was used as a loading control. (e-i) Saline (bleomycin -) or bleomycin (+) was administered to wild type (*Mavs+/+*) and MAVS null mutant (*Mavs-/-*) mice. In order to evaluate the time-kinetics of cellular senescence markers, from whole lung tissues at the indicated time points after bleomycin administration *in vivo*, the expression levels of (e) $P16^{INK4a}$, (f) $P19^{ARF}$ and (g) *P21* mRNAs, respectively, were evaluated by qRT-PCR. (h-i) Western blot results of $P16^{INK4a}$ protein from whole lung tissue lysates at indicated time points after bleomycin administration *in vivo* are presented. β-Actin was used as a loading control. Data are the mean ± SD (b-d) or SEM (e-g). Statistical significance was determined using the 2-way ANOVA with Tukey's multiple comparisons test (b,c, and e-g). **, $P < 0.01$; ***, $P < 0.001$; ****, $P < 0.0001$.

Table S1. Primers used in this study for qRT-PCR.

Gene	Forward primer (5'→3')	Reverse primer (5'→3')
CD206	CTCTGTTCAGCTATTGGACGC	CGGAATTTCTGGGATTCAGCTTC
Arg1	CTCCAAGCCAAAGTCCTTAGAG	AGGAGCTGTCATTAGGGACATC
CD163	ATGGGTGGACACAGAATGGTT	CAGGAGCGTTAGTGACAGCAG
Fizz1	CCAATCCAGCTAACTATCCCTCC	CCAGTCAACGAGTAAGCACAG
IL-10	GCTCTTACTGACTGGCATGAG	CGCAGCTCTAGGAGCATGTG
iNOS	GTTCTCAGCCCAACAATACAAGA	GTGGACGGGTCGATGTCAC
Fibronectin	GCTCAGCAAATCGTGCAGC	CTAGGTAGGTCCGTTCCCACT
α-SMA	GTCCCAGACATCAGGGAGTAA	TCGGATACTTCAGCGTCAGGA
Col1α	GCTCCTCTTAGGGGCCACT	CCACGTCTCACCATTGGGG
Tgfbr1	TCTGCATTGCACTTATGCTGA	AAAGGGCGATCTAGTGATGGA
Tgfbr2	CCGCTGCATATCGTCCTGTG	AGTGGATGGATGGTCCTATTACA
Dab2	CCTTCATTGCTCGTGATGTGA	CCCCAAACAAATCCATCTGGTC
Hgs	TTCGAGCGTCTCCTAGACAAA	GCTTGTGTGTCCCCCTGAC
Il13	CCTGGCTCTTGCTTGCCTT	GGTCTTGTGTGATGTTGCTCA
Ctgf	GGGCCTCTTCTGCGATTTC	ATCCAGGCAAGTGCATTGGTA
Sting	GGTCACCGCTCCAAATATGTAG	CAGTAGTCCAAGTTCGTGCGA
P2rx7	GACAAACAAAGTCACCCGGAT	CGCTCACCAAAGCAAAGCTAAT
P2ry2	CTGGAACCCTGGAATAGCACC	CACACCACGCCATAGGACA
Hmgb1	GGCGAGCATCCTGGCTTATC	GGCTGCTTGTCATCTGCTG
Nlrp3	ATTACCCGCCCGAGAAAGG	TCGCAGCAAAGATCCACACAG
P16INK4a	CCCAACGCCCCGAACT	GCAGAAGAGCTGCTACGTGAA
P19ARF	GCCGCACCGGAATCCT	TTGAGCAGAAGAGCTGCTACGT
P21	CCTGGTGATGTCCGACCTG	CCATGAGCGCATCGCAATC
Rig-I	AAGAGCCAGAGTGTCAGAATCT	AGCTCCAGTTGGTAATTTCTTGG
18s	GTAACCCGTTGAACCCCATT	CCATCCAATCGGTAGTAGCG

Table S2. Antibodies used in this study for Western blot

Antibodies	Source	Identifier
Rabbit polyclonal anti-MAVS (Rodent Specific)	Cell signaling technology	Cat# 4983, RRID:AB_823566
Rabbit monoclonal anti-cGAS (D3O8O) (Mouse Specific)		Cat# 31659, RRID:AB_2799008
Rabbit monoclonal anti-STING (D2P2F)		Cat# 13647, RRID:AB_2732796
Rabbit monoclonal anti-VDAC (D73D12) (HRP Conjugate)		Cat# 12454, RRID:AB_2797922
Rabbit monoclonal anti-Phospho-Smad2 (Ser465/467)/Smad3 (Ser423/425) (D27F4)		Cat# 8828, RRID:AB_2631089
Rabbit monoclonal anti-Smad2/3 (D7G7)		Cat# 8685, RRID:AB_10889933
Rabbit monoclonal anti-Phospho-Smad1 (Ser463/465)/ Smad5 (Ser463/465)/ Smad9 (Ser465/467) (D5B10)		Cat# 13820, RRID:AB_2493181
Rabbit monoclonal anti-Smad1 (D59D7)		Cat# 6944, RRID:AB_10858882
Rabbit monoclonal anti-Cleaved Caspase-3 (Asp175) (5A1E)		Cat# 9664, RRID:AB_2070042
Mouse monoclonal anti-MAVS (E-6)	Santa cruz biotechnology	Cat# sc-365334, RRID:AB_10842299
Mouse monoclonal anti-COL1A		Cat# sc-59772, RRID:AB_1121787
Mouse monoclonal anti-β-Actin (HRP Conjugate)		Cat# sc-47778, RRID:AB_2714189
Mouse monoclonal anti-Fibronectin (EP5)		Cat# sc-8422, RRID:AB_627598
Mouse monoclonal anti MAVS (E-6)-Alexa fluor 647		Cat# sc-365334, RRID:AB_10842299
normal mouse IgG1-Alexa fluor 647		Cat# sc-24636, RRID:AB_737215
Rabbit polyclonal anti-MAVS	Proteintech	Cat# 14341-1-AP, RRID:AB_10548408
Mouse monoclonal anti-Total OXPHOS cocktail (Rodent Specific)	Abcam	Cat# ab110413, RRID:AB_2629281
Rabbit polyclonal anti-alpha smooth muscle actin		Cat# ab5694, RRID:AB_2223021
Mouse monoclonal anti-CD68		Cat# ab955, RRID:AB_307338
Rabbit monoclonal anti-CDKN2A/p16INK4a		Cat# ab211542
Donkey anti-Mouse IgG (H+L) Highly Cross-Adsorbed Secondary Antibody, Alexa Fluor 546	Thermo Fisher Scientific	Cat# A10036, RRID:AB_253401
Donkey anti-Rabbit IgG (H+L) Highly Cross-Adsorbed Secondary Antibody, Alexa Fluor 488		Cat# A-21206, RRID:AB_2535792
Alexa Fluor 700 anti-mouse CD45	Biolegend	Cat# 103128, RRID:AB_493715
PE anti-mouse CD31		Cat# 102408, RRID:AB_312903
Brilliant Violet 605 anti-mouse CD326 (EpCAM)		Cat# 118227, RRID:AB_2563984
PE-Cy7 anti-mouse CD49e		Cat# 103815, RRID:AB_2734164
Pacific Blue anti-mouse F4/80		Cat# 123123, RRID:AB_893487

Materials and Methods

Sircol assay

Collagen contents were determined by quantifying total soluble collagen using the Sircol collagen assay kit (Biocolor, Accurate Chemical & Scientific Corp) according to the manufacturer's instructions. Briefly, 1,000 µl of Sirius red dye reagent were added to 100 µl of the supernatant from lung homogenate, mixed for 30 min, and centrifuged at 12,000 g for 10 min. Pellets were then washed with wash reagent. Finally, pellets were dissolved in 750 µl of alkali reagent, and the amount of collagen was measured using a standard curve for collagen provided by the manufacturer. All assays were done in triplicate.

Flow cytometric analysis.

Murine lungs were cut into small pieces and digested with collagenase (1 mg/ml) and DNase I (30 ug/ml) in RPMI 1640 medium for 20 minutes at 37°C. Digested lungs were passed through 100-µm sterile strainer (Thermo fisher scientific) to obtain a single-cell suspension. The remaining red blood cells were lysed using ACK lysing buffer (Gibco). The Cells were stained with a mixture of fluorochrome-conjugated monoclonal antibodies; mouse anti-CD45-Alexa Fluor 700, anti-CD31-PE, anti-F4/80-Pacific blue, anti-EpCAM-BV 605, anti-CD49e-PE-Cy7. All surface markers were purchased from eBioscience (San Diego, CA, USA). Intracellular MAVS staining was performed using an Intracellular Fixation and Permeabilization kit according to the manufacturer's instructions (eBioscience, San Diego, CA, USA) and stained with MAVS-Alexa Fluor 647 (Santa Cruz Biotechnology) and normal mouse IgG1 Alexa fluor 647 (Invitrogen). Multi-parameter data were acquired on a LSRII flow cytometer (BD) and analyzed using FlowJo software.

Histology, immunohistochemistry and immunofluorescence

Left-lung was inflated with 0.5% low temperature–melting agarose at a constant pressure of 25 cm. The tissues were then fixed overnight with 10% neutral buffered formalin solution, embedded in paraffin, and sectioned for staining with hematoxylin and eosin or Masson's trichrome to assess morphometry or detection of fibrosis, respectively. Semiquantitative scoring of lung fibrosis was performed according to the method of ASHCROFT et al. [1], with minor modifications [2, 3]. Three lung tissue sections collected from each mouse were analyzed. Degrees of pulmonary fibrosis were graded on a scale of 0 – 5: 0, normal lung; 1, minimal areas of inflammation, epithelial hyperplasia and fibrosis, usually limited to subpleural foci in just 1 or 2 section; 2, more frequent lesions; 3, all three sections exhibit lung lesions which are not limited to subpleural foci; 4, extensive lesions in at least 2 or 3 sections; 5, majority of each of three lung sections affected by fibrosis. Immunohistochemistry was performed as previously described [4]. Briefly, 5 μm sections were deparaffinized and rehydrated. After the antigen was recovered by high-pressure heating with Target Retrieval Solution (DakoCytomation), tissues were incubated with different antibody at 4°C overnight and HRP-secondary antibodies (DakoCytomation) for 30 min and then incubated and developed using DAB solution (DakoCytomation). The specific antibodies for MAVS (Cell signaling) and type I collagen (Abcam) were used for staining. Tissue sections were counterstained with hematoxylin. For immunofluoresence staining, sections were incubated with the following primary antibodies: CD68 (Abcam), MAVS (Cell signaling), Alexa Fluor 488–conjugated and Alexa Fluor 546–conjugated secondary antibodies (Thermo fisher scientific). The stained tissues were photographed with a Zeiss LSM 710 confocal microscope.

Terminal deoxynucleotidyltransferase-mediated deoxyuridine triphosphate nick end-labelling (TUNEL) assay

Apoptotic cells were detected in the paraffin embedded lung sections using a TUNEL kit (Abcam, Cambridge, UK), according to the manufacture's protocols. DAB-stained sample slides were counterstained by methyl blue. The quantification of TUNEL-positive cells was performed by QuPath software 2.1 (https://qupath.github.io).

Isolation of murine alveolar macrophages.

Primary mouse alveolar macrophages were obtained from BAL of *Mavs*$^{+/+}$ and *Mavs*$^{-/-}$ mice. The percentage of macrophage lineage (CD45^{+}F4/80^{+}) cells in the living cells isolated from BAL was above 90% by flow cytometry analysis. For macrophage activation experiments, BAL cells were cultured in RPMI1640 media with 10% FBS and 1x penicillin/streptomycin and were seeded 5×10^5 cells per well in 6-well plate. The cells were stimulated with mouse recombinant IFN-γ (100 ng/ml), IL-4 (20 ng/ml) and TGF-β1 (20 ng/ml), respectively, for 18 h. BAL samples from 5 mice in each group were pooled.

ELISA

Each BAL fluid sample was centrifuged, and the supernatants were stored at –70°C until used. The level of TGF-β1 in BALF were measured with DuoSet kit ELISA kits (R&D Systems) according to the manufacturers' instructions.

qRT-PCR

Total RNA was extracted from the lung tissues using RNeasy kit (QIAGEN) and stored at -80°C until reverse transcription. Total RNA was quantified by quantitative PCR using Nanodrop (Life Technologies). The sequences for the primers are given in Table 1 and the cDNA was analyzed by SYBR-Green Supermix (Bio-rad) with an ABI 7500 fast real-time PCR (Applied Biosystems) and normalized to 18S expression. Data are expressed in relative fold change. Primer information is listed in Table S1.

Western blot analysis

The lung tissues were lysed in lysis buffer containing protease/phosphatase inhibitors (GenDEPOT). The soluble fraction was separated by centrifugations at 13,000 × g for 10 min at 4°C. The concentration of total protein in the cleared lysate was measured using a BCA Assay kit (Thermo). The samples were resolved in SDS-PAGE and analyzed by various antibodies as listed in Table S2. The samples were analyzed three times in independent blots. The quantification of protein expression was carried out by optical densitometry and analyzed using the ImageJ software (ImageJ 1.53v, National Institutes of Health, MD, USA).

Quantification of cell-free double-stranded DNA

Cell-free double-stranded DNA (dsDNA) was quantified in the BAL fluid using Quant-iTPicoGreen dsDNA reagent (Thermo), according to the manufacturer's protocol.

Mitochondrial isolation

Mitochondria was isolated using Qproteome mitochondrial isolation kit (Qiagen) according to the manufacturer’s instruction. Briefly, lung tissue was harvested in lysis buffer and

homogenized using a dounce homogenizer, and then centrifuged at 1,000 g for 10 min at 4°C. The pellet was disrupted by ten passages through a 23-gauge needle and then centrifuged at 1,000 g for 10 min at 4°C. The resulting supernatant was further centrifuged at 8,000 g for 15 min at 4°C. The pellet was then washed and kept as the mitochondrial fraction.

Blue Native-Polyacrylamide Gel Electrophoresis (BN-PAGE) and Semi-Denaturing Detergent-Agarose Gel Electrophoresis (SDD-AGE)

MAVS aggregation was evaluated by BN-PAGE or SDD-AGE, respectively, as described previously [5]. Briefly, for BN-PAGE, 20 μg of crude mitochondria was solubilized with 1% digitonin (Sigma) and proteins were separated using a 3-12% Bis-Tris system (Invitrogen). Samples were then transferred to a PVDF membrane for immunoblotting. SDD-AGE was performed according to a published protocol with minor modifications [6]. Briefly, crude mitochondria were resuspended in 1 × sample buffer (50 mM Tris/HCL, 5% glycerol, 2% SDS, and 0.0025% bromophenol blue), and loaded onto a vertical 1.5% agarose gel. After electrophoresis in the running buffer (20 mM Tris, 200 mM Glycine and 0.1% SDS) for 60 minutes with a constant voltage of 100 V at 4°C, the proteins were transferred to a PVDF membrane for immunoblotting.

***In vitro* cell culture**

Mouse lung epithelial cell line (MLE-12) was purchased from ATCC and cultured in DMEM (Gibco) supplemented with 10% FBS (Gibco) and penicillin–streptomycin (Gibco) at 37°C in 5% CO_2. Normal human lung fibroblasts (NHLF) were purchased from Lonza Walkersville Inc. (Walkersville, MD) and were cultured in DMEM with fibroblast growth kit-low serum (ATCC).

NHLF was used between passages 4 and 8. For the treatment with bleomycin *in vitro*, the concentration (10-50 mU/ml) was selected following the publication reported by our group [7].

Isolation and culture of mouse lung fibroblasts and mouse embryonic fibroblasts

Primary mouse lung fibroblasts (MLFs) were isolated from the lungs obtained from C57BL/6J wild-type mice and maintained in DMEM supplemented with 10% FBS and penicillin–streptomycin. MLFs were isolated using a method described previously [8]. Briefly, mouse lungs were minced into 1- to 2-mm^3 pieces and incubated in calcium- and magnesium-free Hanks' balanced salt solution (HBSS) containing 1,000 U/ml collagenase A for 30 min, and after washing with HBSS, then add 0.25% trypsin-EDTA for 20 min at 37°C with shaking. The dissociated cells were centrifuged and cultured in DMEM supplemented with 10% FBS for 1 h, and then adherent fibroblasts were rinsed with HBSS and cultured in DMEM supplemented with 10% FBS and penicillin–streptomycin. MLFs were used between passages 3 and 6. Mouse embryonic fibroblasts (MEF) cells were derived from C57BL/6J wild-type mouse embryos at day 13 following standard procedures, as described previously [9]. MEF cells were maintained in DMEM (Gibco) supplemented with 10% FBS (Gibco) and penicillin–streptomycin (Gibco). All the experiments using MEF cells were done at passage 4-6.

Cell viability assay

The cell viability was measured with the XTT cell viability kit (Cell signaling), according to the manufacturer's instruction.

SA-β-Galactosidase Staining

The evaluation for senescence cells was carried out using a SA-β-Galactosidase staining kit (Cell signaling), according to the manufacturer's instructions. Briefly, cells were seeded in 6-well plates in triplicate. After senescence induction using bleomycin, the cells were fixed with β-Gal Fixative and stained with complete β-Gal Stain Solution. MLE-12 and MEF cells were visualized using a bright-field microscope at x10 or x20 magnification, respectively. The quantification of SA-β-gal-positive cells was assessed in 5 randomly-selected fields per individual sample using ImageJ software (ImageJ 1.53v, National Institutes of Health, MD, USA).

References

1. Ashcroft T, Simpson JM, Timbrell V. Simple method of estimating severity of pulmonary fibrosis on a numerical scale. *J Clin Pathol* 1988: 41(4): 467-470.
2. Izbicki G, Segel MJ, Christensen TG, Conner MW, Breuer R. Time course of bleomycin-induced lung fibrosis. *Int J Exp Pathol* 2002: 83(3): 111-119.
3. Matsuse T, Teramoto S, Katayama H, Sudo E, Ekimoto H, Mitsuhashi H, Uejima Y, Fukuchi Y, Ouchi Y. ICAM-1 mediates lung leukocyte recruitment but not pulmonary fibrosis in a murine model of bleomycin-induced lung injury. *The European respiratory journal : official journal of the European Society for Clinical Respiratory Physiology* 1999: 13(1): 71-77.
4. Ma B, Kang MJ, Lee CG, Chapoval S, Liu W, Chen Q, Coyle AJ, Lora JM, Picarella D, Homer RJ, Elias JA. Role of CCR5 in IFN-gamma-induced and cigarette smoke-induced emphysema. *The Journal of clinical investigation* 2005: 115(12): 3460-3472.
5. Wittig I, Braun HP, Schagger H. Blue native PAGE. *Nat Protoc* 2006: 1(1): 418-428.
6. Bagriantsev SN, Kushnirov VV, Liebman SW. Analysis of amyloid aggregates using agarose gel electrophoresis. *Methods in enzymology* 2006: 412: 33-48.
7. Yu G, Tzouvelekis A, Wang R, Herazo-Maya JD, Ibarra GH, Srivastava A, de Castro JPW, DeIuliis G, Ahangari F, Woolard T, Aurelien N, Arrojo EDR, Gan Y, Graham M, Liu X, Homer RJ, Scanlan TS, Mannam P, Lee PJ, Herzog EL, Bianco AC, Kaminski N. Thyroid hormone

inhibits lung fibrosis in mice by improving epithelial mitochondrial function. *Nat Med* 2018: 24(1): 39-49.

8. Edelman BL, Redente EF. Isolation and Characterization of Mouse Fibroblasts. *Methods in molecular biology (Clifton, NJ)* 2018: 1809: 59-67.

9. Jozefczuk J, Drews K, Adjaye J. Preparation of mouse embryonic fibroblast cells suitable for culturing human embryonic and induced pluripotent stem cells. *Journal of visualized experiments : JoVE* 2012(64).